Pairing and rotational properties of actinides and superheavy nuclei in covariant density functional theory

A. V. Afanasjev and O. Abdurazakov
Department of Physics and Astronomy, Mississippi State University, Mississippi 39762, USA
(Received 21 February 2013; revised manuscript received 29 June 2013; published 22 July 2013)

The cranked relativistic Hartree-Bogoliubov theory has been applied for a systematic study of pairing and rotational properties of actinides and light superheavy nuclei. Pairing correlations are taken into account by the Brink-Booker part of finite-range Gogny D1S force. For the first time, in the covariant density functional theory (CDFT) framework, the pairing properties of deformed nuclei are studied via the quantities (such as three-point $\Delta^{(3)}$ indicators) related to odd-even mass staggerings. The investigation of the moments of inertia at low spin and the $\Delta^{(3)}$ indicators shows the need for an attenuation of the strength of the Brink-Booker part of the Gogny D1S force in pairing channel. The investigation of rotational properties of even-even and odd-mass nuclei at normal deformation, performed in the density functional theory framework in such a systematic way for the first time, reveals that in the majority of the cases the experimental data are well described. These include the evolution of the moments of inertia with spin, band crossings in the $A \geqslant 242$ nuclei, the impact of the particle in specific orbital on the moments of inertia in odd-mass nuclei. The analysis of the discrepancies between theory and experiment in the band crossing region of $A \leqslant 240$ nuclei suggests the stabilization of octupole deformation at high spin, not included in the present calculations. The evolution of pairing with deformation, which is important for the fission barriers, has been investigated via the analysis of the moments of inertia in the superdeformed minimum. The dependence of the results on the CDFT parametrization has been studied by comparing the results of the calculations obtained with the NL1 and NL3* parametrizations.

DOI: 10.1103/PhysRevC.88.014320 PACS number(s): 21.10.Pc, 21.30.Fe, 21.60.Jz, 27.90.+b

I. INTRODUCTION

Starting from the dawn of the 21st century, there is an increased interest in a detailed spectroscopic study of the heaviest actinides and light superheavy nuclei. Rotational, single-particle and other properties of these nuclei were and are studied both in experiment and in theory (see Refs. [1,2] and references therein). There is a hope that detailed spectroscopic information on such nuclei will allow us to better test and constrain theoretical models so that the location of the island of enhanced stability of spherical superheavy nuclei can be predicted with a higher level of confidence.

A continuing experimental effort to study rotational properties of such nuclei is driven in part by the fact that in odd-mass nuclei they provide an important additional fingerprint for the Nilsson configuration assignment for the bandheads on which the rotational structures are built [3]. The investigation of high-spin structures also provides important information on stability of nuclei against fission [4]. Among recent surprises is the observation of a rotational band in the $Z = 104$ ^{256}Rf nucleus up to very high spin of $I = 20^{+}$ [5]; this is the highest-Z nucleus is which such structures were observed. In addition, there is a revival of theoretical interest in the description of such structures. This is illustrated by recent systematic investigations of rotational properties in heavy actinides and light superheavy nuclei performed within a total Routhian surface (TRS) approach [6] and a particle-number conserving method based on a cranked shell model (PNC + CSM) [7,8]. These approaches are based on phenomenological Woods-Saxon and Nilsson potentials, respectively.

Alternative and more microscopic approaches are based on nonrelativistic and relativistic density functional theories (DFT) [9,10]. Unfortunately, these approaches[1] were only occasionally used for the description of rotational structures in the pairing regime and no systematic assessment of their errors and the sources of these errors are available. It turns out that within these approaches more efforts were dedicated to the investigation of superdeformed (SD) rotational bands in different mass regions (see Refs. [9,10] and references therein) than to the study of rotational bands at normal deformation. However, in contrast with normal-deformed (ND) bands, neither spin nor parity are known for absolute majority of the SD bands. The studies of the ND bands over observable frequency ranges have been performed only in a few nuclei within the cranked Hartree(+Fock)+Bogoliubov (HB or HFB) frameworks based on DFT. These are ^{72,74,76}Kr [14], ^{74}Rb [15], ^{76}Sr [16], and ^{80}Zr [14] studied in covariant DFT (CDFT) as well as ^{48,50}Cr [19]; a few even-even Er and Yb nuclei [17–19]; and ^{240}Pu [18] studied in Gogny DFT (GDFT). Somewhat more attention has been paid to rotational structures of actinides within Skyrme DFT (SDFT) [20,21], but even these investigations are far from being systematic.

The situation is even worse in odd-mass nuclei where only a few rotational bands across the nuclear chart have been studied in the DFT framework so far (see Sec. V for a detailed overview). However, rotational properties of one-quasiparticle configurations give important information on their underlying structure, thus providing an extra tool for a configuration assignment. This is especially important

[1]We consider here only the calculations which include approximate particle number projection since it is needed for a proper description of rotational properties [11–13].

for light superheavy nuclei at the edge of the region where spectroscopic studies are still feasible (the nuclei with masses $A \sim 255$ and proton number $Z \geqslant 102$) [3] since alternative methods of configuration assignment are either unreliable and/or questionable or cannot be employed because of the limitations of the experimental measurements.

Covariant density functional theory [10] is well suited for the description of rotational structures. It exploits basic properties of QCD at low energies, in particular symmetries and the separation of scales [22]. Built on the Dirac equation, it provides a consistent treatment of the spin degrees of freedom [22,23] and spin-orbit splittings [24,25]; the latter has an essential influence on the underlying shell structure. It also includes the complicated interplay between the large Lorentz scalar and vector self-energies induced on the QCD level by the in-medium changes of the scalar and vector quark condensates [23]. Lorentz covariance of CDFT leads to the fact that time-odd mean fields of this theory are determined as spatial components of Lorentz vectors and therefore coupled with the same constants as the timelike components [26], which are fitted to ground-state properties of finite nuclei. This is important for the description of odd-mass nuclei [26], the excitations with unsaturated spins, magnetic moments [25], and nuclear rotations [10,27,28]. The successes of the CDFT in the description of rotating nuclei both in paired and unpaired regimes and at different extremes {superdeformation (see Ref. [10] and references therein), ultrahigh spins [29] and the limits of angular momentum in nuclear configurations [10,30]} are well documented.

One should note that our understanding of the pairing properties in the CDFT framework is far from being satisfactory. Although it has been shown in Ref. [31] that a relativistic bare potential (Bonn potential) reproduces pairing correlations at the Fermi surface in the CDFT application to infinite nuclear matter, its mathematical properties make a numerical solution of the relativistic Hartree + Bogoliubov (RHB) equations with this potential in the pairing channel extremely difficult task. This task has not been solved so far. On the other side, the relativity does not affect pairing significantly [32]. As a consequence, simpler versions of phenomenological nonrelativistic pairing such as constant gap pairing, monopole pairing, zero-range δ-pairing (see Ref. [33] and references therein), separable pairing [34], and the pairing based on the Brink-Booker part of finite-range Gogny force [13,35] are used in the CDFT calculations.

In all CDFT applications of the first three types of pairing the selection of the pairing strength has been guided either by nonrelativistic results (see, for example, Refs. [33,36]) or by the local fits to experimental or empirical pairing gaps (see, for example, Ref. [37]). The strengths of separable pairing have been fitted to the properties of the Brink-Booker parts of finite-range Gogny D1S and D1 forces in nuclear matter [34]. However, to our knowledge, the results of the calculations with these types of pairing have not been directly confronted with experimental observables sensitive to pairing such as the moments of inertia and/or the indicators related to odd-even mass staggerings (such as three-point $\Delta^{(3)}$ indicators, see Sec. III D below for details). Thus, at present, it is not clear how accurately these types of pairing perform. Global investigations of the pairing in the CDFT framework that are similar to those performed in the nonrelativistic SDFT framework (see Refs. [38,39]) are not available yet.

Somewhat more is known in the CDFT about the properties of the pairing force based on the Brink-Booker part of the finite-range Gogny D1S force via the studies of rotational structures. Available investigations within the cranked RHB theory with approximate particle number projection by means of the Lipkin-Nogami method (CRHB + LN) show that it performs rather well in nuclei with masses $A \leqslant 200$ [10,13,14,40], but its strength has to be decreased by approximately 10% in actinides [1]. On the contrary, available applications of the RHB theory with pairing force based on the Brink-Booker part of finite-range Gogny D1S force in pairing channel to the ground-state properties across the nuclear chart follow the prescription of Ref. [35], in which the strength of the Brink-Booker part is increased by a factor of 1.15. This difference in the selection of the pairing strength definitely requires clarification.

To our knowledge, the detailed analysis of pairing indicators (such as the $\Delta^{(3)}$ indicators) has not been performed so far in the relativistic mean field + BCS, RHB or CRHB(+LN) frameworks because of the complexity of the definition of the ground states in odd-mass nuclei. In order to define the ground state in odd-mass nucleus, the binding energies have to be calculated for a number of one-quasiparticle configurations based on the orbitals active in the vicinity of the Fermi level and only then the lowest in energy state is assigned to the ground state. This nontrivial problem has been solved, first, for only a few nuclei in Ref. [1] and then in the systematic studies of actinides and rare-earth nuclei in Ref. [41].

The current paper aims to provide a detailed and systematic study of the pairing properties of actinides in the RHB and CRHB(+LN) frameworks via simultaneous investigation of the moments of inertia and the $\Delta^{(3)}$ indicators. Such an investigation covers not only normal-deformed but also superdeformed structures. The rotational structures in the SD minimum provide only available information on the evolution of pairing with deformation in actinides. This is important for an understanding of fission barriers which, according to Ref. [33], sensitively depend on the pairing properties. In addition, the rotational properties of even-even and odd-mass actinides are studied in a systematic way up to high spin in order to see the typical accuracy of the description of rotational and band crossing features, the impact of blocked orbital on rotational properties, and the feasibility of the use of rotational features in configuration assignment of light odd-mass superheavy nuclei. The systematic analysis is restricted to reflection symmetric nuclei. As a consequence, light octupole deformed actinides [42] are omitted. Based on the results obtained in actinides, the deformation and rotational properties of superheavy nuclei are also studied.

The manuscript is organized as follows. The CRHB(+LN) theory and its details are discussed in Sec. II. Section III is devoted to the pairing properties of actinides. In this section, the pairing strength is defined and the calculated deformation, low-spin rotational properties and the $\Delta^{(3)}$ indicators are compared with experiment. Rotational properties of even-even and odd-mass nuclei are considered up to high spin

in Secs. IV and V, respectively. Deformation, pairing and rotational properties of actinide fission isomers are discussed in Sec. VI. We report the results for deformation and rotational properties of even-even superheavy nuclei in Sec. VII. Finally, Sec. VIII summarizes the results of our work.

II. THEORETICAL FORMALISM

The CRHB + LN equations for the fermions in the rotating frame (in one-dimensional cranking approximation) are given by [13]

$$\begin{pmatrix} \hat{h}'_D - \lambda' - \Omega_x \hat{J}_x & \hat{\Delta} \\ -\hat{\Delta}^* & -\hat{h}'^*_D + \lambda' + \Omega_x \hat{J}_x{}^* \end{pmatrix} \begin{pmatrix} U(\boldsymbol{r}) \\ V(\boldsymbol{r}) \end{pmatrix}_k = E'_k \begin{pmatrix} U(\boldsymbol{r}) \\ V(\boldsymbol{r}) \end{pmatrix}_k, \tag{1}$$

where

$$\hat{h}'_D = \hat{h}_D + 4\lambda_2\rho - 2\lambda_2 \mathrm{Tr}(\rho), \tag{2}$$

$$\lambda' = \lambda_1 + 2\lambda_2, \tag{3}$$

$$E'_k = E_k - \lambda_2, \tag{4}$$

where $\hat{h}_D$ is the Dirac Hamiltonian for the nucleon with mass m, λ_1 is defined from the average particle number constraints for protons and neutrons, $\rho_\tau = V^*_\tau V^T_\tau$ is the density matrix, $U_k(\boldsymbol{r})$ and $V_k(\boldsymbol{r})$ are quasiparticle Dirac spinors, E_k denotes the quasiparticle energies, and $\hat{J}_x$ is the angular-momentum component. The LN method corresponds to a restricted variation of $\lambda_2\langle(\Delta N)^2\rangle$ (see Ref. [13] for definitions of λ_1 and λ_2), where λ_2 is calculated self-consistently in each step of the iteration. The form of the CRHB + LN equations given above corresponds to the shift of the LN modification into the particle-hole channel.

The Dirac Hamiltonian $\hat{h}_D$ contains an attractive scalar potential $S(\boldsymbol{r})$,

$$S(\boldsymbol{r}) = g_\sigma \sigma(\boldsymbol{r}), \tag{5}$$

a repulsive vector potential $V_0(\boldsymbol{r})$,

$$V_0(\boldsymbol{r}) = g_\omega \omega_0(\boldsymbol{r}) + g_\rho \tau_3 \rho_0(\boldsymbol{r}) + e\frac{1-\tau_3}{2} A_0(\boldsymbol{r}), \tag{6}$$

and a magnetic potential $\boldsymbol{V}(\boldsymbol{r})$,

$$\boldsymbol{V}(\boldsymbol{r}) = g_\omega \boldsymbol{\omega}(\boldsymbol{r}) + g_\rho \tau_3 \boldsymbol{\rho}(\boldsymbol{r}) + e\frac{1-\tau_3}{2} \boldsymbol{A}(\boldsymbol{r}). \tag{7}$$

The last term breaks time-reversal symmetry and induces currents. In rotating nuclei, the time-reversal symmetry is broken by the Coriolis field. Without rotation, it is broken when the time-reversal orbitals are not occupied pairwise. In the Dirac equation, the spacelike components of the vector mesons $\boldsymbol{\omega}(\boldsymbol{r})$ and $\boldsymbol{\rho}(\boldsymbol{r})$ have the same structure as the spacelike component $\boldsymbol{A}(\boldsymbol{r})$ generated by the photons. Since $\boldsymbol{A}(\boldsymbol{r})$ is the vector potential of the magnetic field, by analogy the effect due to presence of the vector field $\boldsymbol{V}(\boldsymbol{r})$ is called *nuclear magnetism* [43]. It has considerable influence on the magnetic moments [44] and the moments of inertia [27,28] and affects the properties of odd- and odd-odd nuclei [26]. In the present calculations the spatial components of the vector mesons are properly taken into account in a fully self-consistent way. The detailed description of the mesonic degrees of freedom in the CRHB + LN theory is presented in Ref. [13].

The CRHB(+LN) equations are solved on the basis of an anisotropic three-dimensional harmonic oscillator in Cartesian coordinates. The same basis deformation $\beta_0 = 0.3$, $\gamma = 0^\circ$ and oscillator frequency $\hbar\omega_0 = 41A^{-1/3}$ MeV were used in the calculations. All fermionic and bosonic states belonging to the shells up to $N_F = 14$ and $N_B = 20$ were taken into account in the normal-deformed minimum in the diagonalization of the Dirac equation and the matrix inversion of the Klein-Gordon equations, respectively. As follows from a detailed analysis of Refs. [1,41], this truncation of the basis provides sufficient accuracy of the calculations. In order to have similar accuracy in the superdeformed minimum, N_F was increased to 16 in the calculations.

The calculations were performed as a function of rotational frequency in the frequency range $\Omega_x = 0.01$–0.45 MeV in steps of 0.02 MeV outside the band crossing regions and 0.01 MeV in the band crossing regions and their vicinities. Note that full convergence is not always obtained at all frequencies; for these frequencies, no calculated curve is shown in the figures below. This typically happens in the regime of extremely week pairing at high rotational frequencies in the $Z = 90$–102 nuclei (see Figs. 10 and 9 below). Alternatively, no convergence takes place in the band crossing region or above of some Rf and Sg nuclei (see Figs. 10 and 9 below), most likely because the solution jumps between two closely lying in energy minima.

The calculations have been performed with the NL1 [45] and NL3* [46] parametrizations of the RMF Lagrangian. The selection of the parametrizations has been dictated by the following considerations:

(i) *The accuracy of the description of single-particle properties*. The description of rotating nuclei is more complicated as compared with that of the ground-state properties (such as binding energies, radii, etc.) of even-even nuclei. This is because it depends not only on the calculated deformations of nuclei but also on the energies and alignment properties of the single-particle orbitals. For example, the alignments of proton or neutron angular momenta in the upbending/backbending region and whether it proceeds smoothly or in a abrupt way strongly depend on the accuracy of the description of the excitation energies of high-j aligning orbitals with respect to the quasiparticle vacuum [47]. So far, the accuracy of the description of deformed one-quasiparticle states has been systematically studied only with the NL1 and NL3* parametrization in Ref. [41]; this study covers all one-quasiparticle states in the actinide region. It is interesting that the overall accuracy of the description of the energies of deformed one-quasiparticle states in Ref. [41] is slightly better in the NL1 parametrization which was fitted 25 years ago, mostly to the nuclei at the β-stability line, than in

the recent NL3* parametrization. This suggests that the inclusion of extra information on neutron-rich nuclei into the fit of the NL3* parametrization may lead to some degradation of the description of single-particle states along the valley of β stability.

So far the calculated alignment properties of single-particle orbitals have only been confronted with experiment in the unpaired regime at normal deformation in the $A \sim 80$ [14] region and at superdeformation in the $A \sim 60$ [48] and 150 [49] mass regions. These investigations have been mostly performed with the NL1 parametrization, which describes well the alignment properties of the single-particle orbitals.

(ii) *The accuracy of the description of the moments of inertia in unpaired regime*. The pairing has a significant impact on the moments of inertia which is much stronger than its impact on other physical observables. As a consequence, it is very difficult to disentangle pairing and rotational alignment contributions to the moments of inertia. Fortunately, the pairing is very weak at high spin and, thus, can be neglected there [10,49,50]. As a result, it becomes possible to benchmark the performance of different CDFT parametrizations with respect to the description of the moments of inertia in unpaired regime.

So far such detailed benchmark calculations across the nuclear chart are available only for the NL1 parametrization. They include the investigations of the moments of inertia of superdeformed bands in the $A \sim 60$ [48] and 150 [10,50] mass regions and in ^{108}Cd [51]. Moreover, the rotational properties of smooth terminating bands in the $A \sim 110$ mass region [10] and triaxial superdeformed bands both at ultrahigh spin in ^{158}Er [29] and at moderate/high spin in the $A \sim 170$ mass region [52] have been successfully studied with this parametrization. These detailed investigations showed that the NL1 parametrization provides a very good description of rotational and deformation properties of studied nuclei which in many cases is similar but frequently better than the one obtained with newer parametrizations such as NL3 and NLSH (for later comparison see Refs. [48,49]). These results give us strong confidence that the NL1 parametrization should perform reasonably well also in actinides.

Limited benchmark calculations in the unpaired regime are available also for the NL3* parametrization but only for a few nuclei (^{58}Cu, ^{143}Eu, ^{109}Sb, and ^{74}Kr [46] and ^{158}Er [29]) across the nuclear chart. However, these studies cover different types of bands such as near-axial and triaxial superdeformed bands and smoothly terminating bands.

(iii) *The accuracy of the description of pairing properties by the Brink-Booker part of the finite-range Gogny D1S force*. As discussed in the Introduction, our knowledge of pairing properties of the Brink-Booker part of Gogny D1S force comes mostly from the CRHB + LN calculations. One interesting observation, born in the studies of few rotational bands, is the need for an attenuation of this pairing force in the nobelium region [1]. To validitate this observation, the systematic calculations of the moments of inertia and the $\Delta^{(3)}$ indicators in actinides have to be confronted with available systematic studies in lighter nuclei employing the same CDFT parametrization. Such studies of the moments of inertia are available only for normal-deformed proton-rich $A \sim 70$ [14] and rare-earth [40] nuclei and for superdeformed nuclei in the $A \sim 190$ region [13]. The later two studies are performed with the NL1 parametrization, while the former one with NL3. However, it was verified that the results for rotational structures in the $A \sim 70$ mass region with the same pairing are similar for the NL1 and NL3 parametrizations.

Thus, two different parametrizations, namely NL1, fitted to the nuclei in the valley of β stability, and NL3*, tailored towards the description of neutron-rich nuclei, are used in the current study. This selection allows us to study the dependence of the results on the CDFT parametrization. In addition, the use of two parametrizations allows us, in many cases, to circumvent the convergence problems for specific blocked orbitals in odd-mass nuclei which can show up in one parametrization but will not affect the solution in another parametrization (see Sec. V for details). For example, the calculations for the moments of inertia of the $\pi 5/2[523]$ and $\pi 3/2[521]$ rotational bands in ^{214}Am are possible only with the NL1 parametrization, while the ones for the $\nu 9/2[734]$ bands in ^{247}Cm and ^{249}Cf are possible only with NL3* (see Figs. 16, 21, and 22 below). Other examples of complementarity of the calculations with NL1 and NL3* can be found in Sec. V.

It is clear that the NL3* parametrization is less tested than the NL1 one in respect to the description of rotating nuclei. However, it has been successfully applied to the description of binding energies [46], ground-state properties of deformed nuclei [53], single-particle spectra of spherical odd-mass nuclei [25], fission barriers [37], giant resonances [46], and breathing mode [54].

The NL1 and NL3* parametrizations are representatives of the meson-exchange models with nonlinear meson-nucleon couplings [55]. This type of model can be supplemented, for example, by isoscalar-isovector coupling as is done in the FSUGold model [56]. There are two other classes of covariant density functional models such as density-dependent meson-exchange [57] (represented, for example, by the DD-ME2 [58] parametrization) and density-dependent point-coupling [59,60] (represented, for example, by the DD-PC1 [61] and PC-PK1 [62] parametrizations) models. However, these parametrizations have not been benchmarked with respect to the description of rotational structures in the unpaired regime and nothing is known about their accuracy of the description of one-quasiparticle deformed states in odd-mass nuclei. Thus, they are not employed in the current study.

Nuclear configurations of deformed odd nuclei [one-quasiparticle (1-qp) configurations] are labeled by means of the asymptotic quantum number $\Omega[Nn_z\Lambda]$ (Nilsson quantum number) of the dominant component of the wave function of blocked single-particle orbital at low rotational frequency.

III. PAIRING PROPERTIES

A. Formalism

The pair field $\hat{\Delta}$ in CRHB(+LN) theory is given by

$$\hat{\Delta} \equiv \Delta_{ab} = \frac{1}{2}\sum_{cd} V^{pp}_{abcd}\kappa_{cd}, \tag{8}$$

where the indices $a, b, \ldots$ denote quantum numbers which specify the single-particle states with the space coordinates $\boldsymbol{r}$, as well as the Dirac and isospin indices s and τ. It contains the pairing tensor κ,

$$\kappa = V^* U^T, \tag{9}$$

and the matrix elements V^{pp}_{abcd} of the effective interaction in the particle-particle (pp) channel, for which the Brink-Booker part of phenomenological nonrelativistic Gogny-type finite-range interaction

$$V^{pp}(1,2) = f\sum_{i=1,2} e^{-[(\boldsymbol{r}_1-\boldsymbol{r}_2)/\mu_i]^2} \times (W_i + B_i P^\sigma - H_i P^\tau - M_i P^\sigma P^\tau) \tag{10}$$

is used. The clear advantage of such a force is that it provides an automatic cutoff of high-momentum components. The motivation for such an approach to the description of pairing is given in Ref. [13]. In Eq. (10), μ_i, W_i, B_i, H_i, and M_i ($i = 1, 2$) are the parameters of the force and P^σ and P^τ are the exchange operators for the spin and isospin variables, respectively. The D1S parametrization of the Gogny force [63,64] is used here. Note that a scaling factor f is introduced in Eq. (10), the role of which is discussed in Sec. III B.

As a measure for the size of the pairing correlations in Hartree(-Fock)-Bogoliubov calculations, we use the pairing energy

$$E_{\text{pairing}} = -\tfrac{1}{2}\text{Tr}(\Delta\kappa). \tag{11}$$

B. The selection of the scaling factor f

In the CRHB + LN framework, the original strength [scaling factor $f = 1.0$ in Eq. (10)] of the Brink-Booker part of the Gogny D1S force provided a good description of the moments of inertia in the $A \sim 75$ [14], $A \sim 160$–170 [40], and $A \sim 190$ [13] mass regions. However, as discussed in detail in Ref. [1], it produces pairing correlations in the $A \sim 250$ mass region that are too strong in the CRHB + LN calculations, and, thus, it has to be attenuated ($f < 1.0$) in order to reproduce the observed moments of inertia. The cranked HFB calculations in the Gogny DFT also show the same problem (see discussion in Sec. III A of Ref. [1]). The need for attenuation of the strength of the Brink-Booker part within the framework of the CRHB + LN theory is not surprising since its pairing properties were adjusted by fitting only the odd-even mass differences of the Sn isotopes [63,64] which are far away from actinides. In addition, this fit was done in the framework of the HFB theory completely based on the Gogny force, while only the Brink-Booker part of the Gogny force is used in the pairing channel of the CRHB + LN theory.

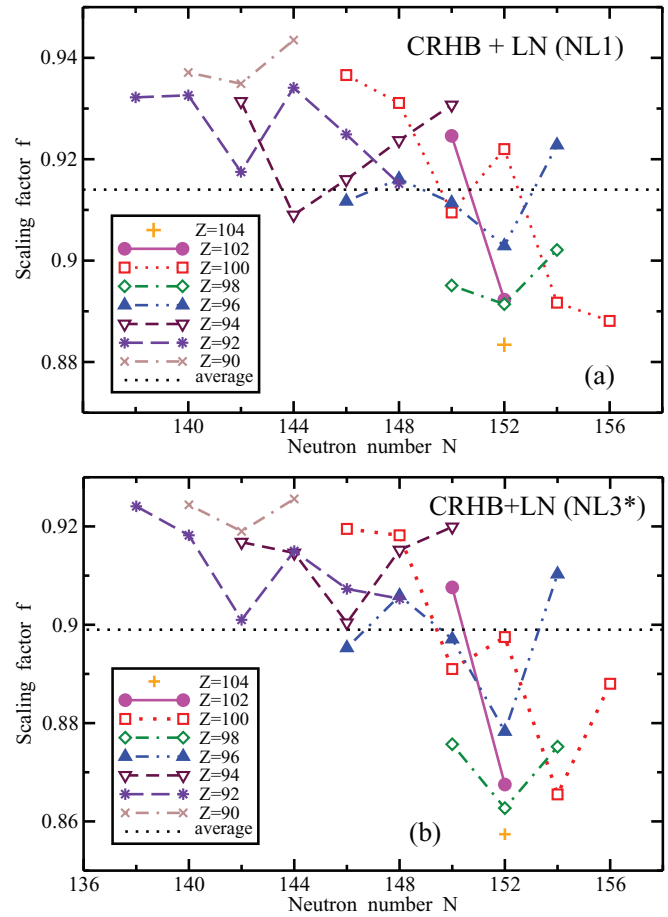

FIG. 1. (Color online) Scaling factors as a function of neutron number for individual nuclei of different isotope chains. The dotted line corresponds to the average scaling factor f_{av} for a given parametrization of the CDFT. The results of the calculations with the NL1 and NL3* parametrizations are presented.

In Ref. [1], the scaling factor f of the Brink-Booker part of finite-range Gogny D1S force [see Eq. (10)] has been chosen to reproduce the experimental kinematic moment of inertia of the ground-state rotational band in ^{254}No at rotational frequency $\Omega_x = 0.15$ MeV. For example, the value $f = 0.893$ has been obtained for the CRHB + LN calculations with the NL1 parametrization (see Table I in Ref. [1]). It provided good description of the moments of inertia of rotational bands in ^{252,254}No [1], ^{250}Fm [65], ^{253}No [66], and ^{255}Lr [67].

However, considering the more systematic character of the current investigation, the scaling factor f has been defined by the fit to the moments of inertia extracted from the $I^\pi = 2^+$ states of ground-state rotational bands in all even-even actinides for which such experimental data were available by the end of June 2012. If not explicitly specified, the experimental data have been taken from Refs. [68,69]; the nuclei used in the fit are shown in Fig. 1. The advantage of such an approach, in which the scaling factor f is defined at very low frequency $\Omega_x \sim 0.02$ MeV, as compared with the one used in Ref. [1], is twofold. First, the definition of scaling factor f in Ref. [1] at $\Omega_x = 0.15$ MeV is affected by the accuracy of the description of the alignments of specific single-particle

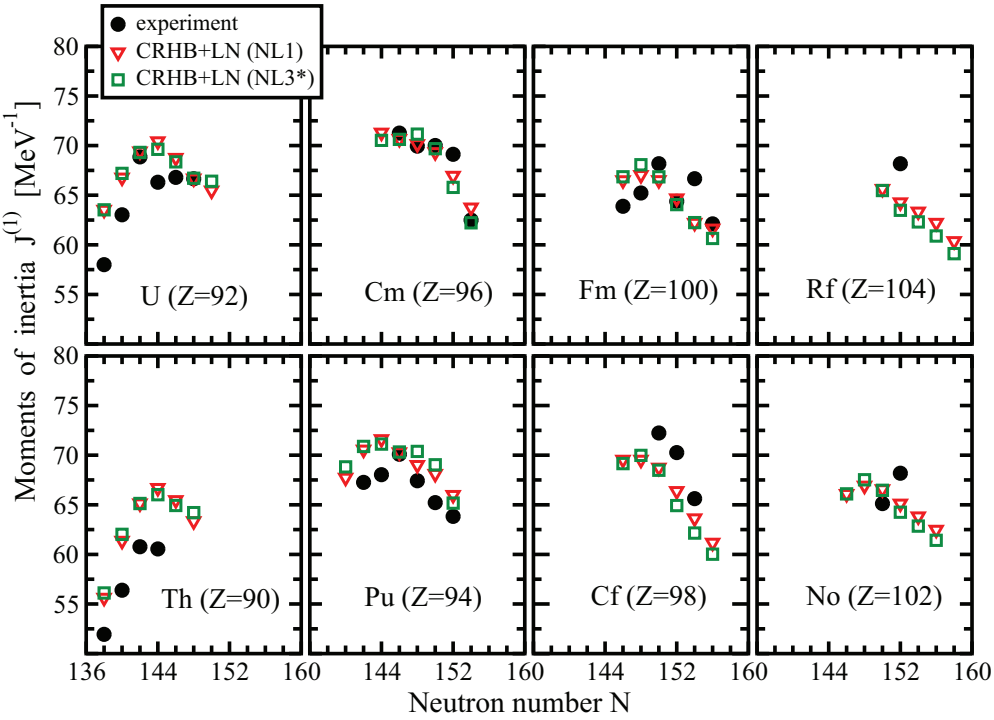

FIG. 2. (Color online) Calculated and experimental moments of inertia at low spin. Experimental moments of inertia are extracted from the energies of the 2^+ states. Calculated values are obtained in the CRHB + LN calculations with $f_{\rm av}$ specific to a given parametrization at the rotational frequency corresponding to experimental energy of the $2^+ \rightarrow 0^+$ transition. Experimental data are shown by filled black circles, while calculated values are shown with red triangles (the NL1 parametrization) and green squares (the NL3* parametrization). Theoretical results are shown at $\Omega_x = 0.02$ MeV in the cases when experimental data are not available.

orbitals (in particular, the ones emerging from proton $i_{13/2}$ and neutron $j_{15/2}$ subshells). This factor affects the definition of f at $\Omega_x = 0.02$ MeV to a much smaller extent. As a result, the current calculations test the predictive power of the model with respect to rotational response in a more straightforward way. Second, such a definition of f allows us to verify whether the fit of pairing strength to the moments of inertia leads to a consistent description of three-point indicators $\Delta^{(3)}$ (extracted from experimental odd-even mass staggerings), which are defined at no rotation.

Figure 1 shows individual scaling factors f_i for the nuclei used in the fit; these factors exactly reproduce the moments of inertia extracted from the 2^+ states of the ground-state rotational bands. In addition, the average scaling factor

$$f_{\rm av} = \frac{\sum_{i=1}^{K} f_i}{K}, \qquad (12)$$

where K is the number of nuclei used in the fit, is shown by dotted lines. The $f_{\rm av}$ is equal to 0.9147 and 0.899 in the NL1 and NL3* parametrizations, respectively. Similarly to Ref. [1] these scaling factors only weakly depend on the CDFT parametrization. For the NL1 parametrization, the obtained value of $f_{\rm av} = 0.9147$ is reasonably close to $f = 0.893$ obtained for ^{254}No in Ref. [1]. These average scaling factors $f_{\rm av}$ will be used in systematic calculations of rotational bands in the actinides and superheavy elements.

C. Rotational and deformation properties at low spin

The kinematic moments of inertia at low spin obtained with average scaling factors $f_{\rm av}$ are shown in Fig. 2. One can see that the moments of inertia are described with an accuracy better than 10%. However, the use of average scaling factors leaves some unresolved trends as a function of particle number in both parametrizations. Figures 1 and 2 show that the pairing has to be slightly weaker (stronger) in the nuclei with high Z and high N (low Z and low N) relative to the calculations performed with $f_{\rm av}$. Similar deviations from experiment exists at low spin also in the CRHB + LN calculations in the rare-earth region (see Fig. 1 in Ref. [40]).

Direct experimental information on the deformations of nuclei from Coulomb excitation and lifetime measurements is quite limited [70]. An alternative method is to derive a quadrupole moment from the $2^+ \rightarrow 0^+$ transition energy by employing the relation given by Grodzins [71] or by later refinements [72]. The prescription of Ref. [72] has an accuracy of about 10%. From the calculated and experimental charge quadrupole moments Q, the deformation parameters β_2 are derived by the relation

$$Q = \sqrt{\frac{16\pi}{5}} \frac{3}{4\pi} Z R_0^2 \beta_2, \quad \text{where} \quad R_0 = 1.2A^{1/3}. \qquad (13)$$

The simple linear expression is used to maintain consistency with earlier papers [70]. It is sufficient for comparison between calculations and experiment because the same relation is used.

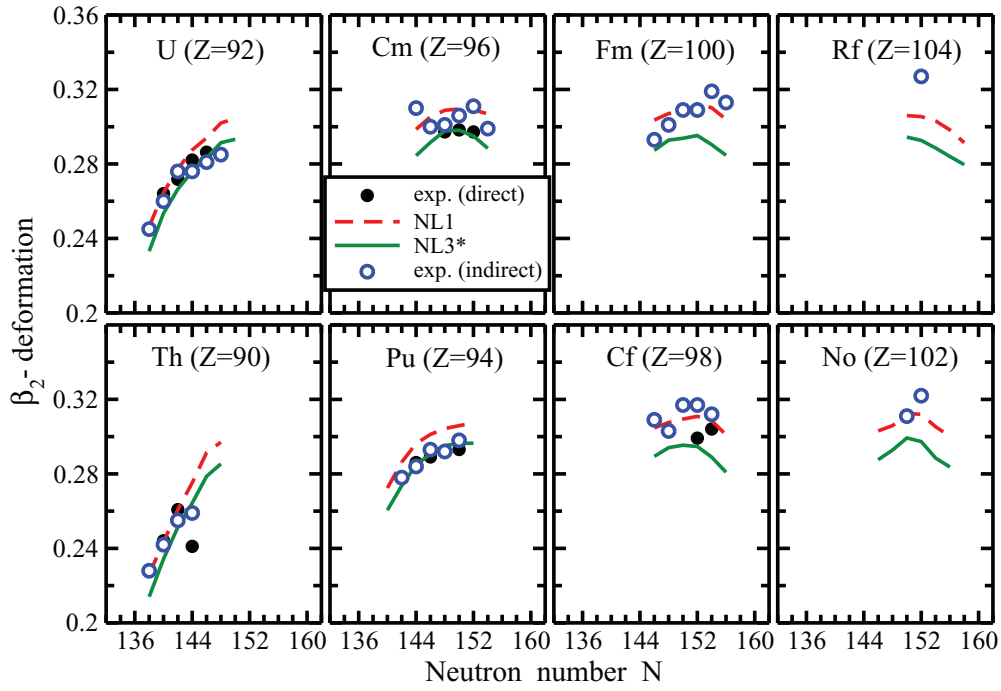

FIG. 3. (Color online) The calculated (lines) and experimental (circles) quadrupole deformation parameters β_2. The experimental values of β_2 obtained in the direct measurements [70] are shown by solid circles, while those deduced from the $2^+ \to 0^+$ transition energies, with the prescription of Ref. [72], are given by open circles. The results of the calculations with the NL1 and NL3* parametrizations are shown by red dashed and green solid lines, respectively.

Including higher powers of β_2, e.g., as in Ref. [73], yields values of β_2 that are $\approx$10% lower.

Experimental quadrupole deformations of the nuclei under study are rather well reproduced in the CRHB + LN calculations (Fig. 3). Thus, they do not represent a major source of the deviations between theory and experiment for kinematic moments of inertia. Considering typical uncertainties of the extraction of quadrupole deformation either in direct [70] or indirect [72] methods, it is difficult to give a preference to either NL1 or NL3* parametrization based on this observable.

D. Three-point indicators $\Delta^{(3)}$

The strength of pairing correlations can also be accessed via the three-point indicator [74]

$$\Delta_\nu^{(3)}(N) = \frac{\pi_N}{2}\left[B(N-1) + B(N+1) - 2B(N)\right], \qquad (14)$$

which is frequently used to quantify the odd-even staggering (OES) of binding energies. Here $\pi_N = (-1)^N$ is the number parity and $B(N)$ is the (negative) binding energy of a system with N particles. In Eq. (14), the number of protons Z is fixed, and N denotes the number of neutrons, i.e., this indicator gives the neutron OES. The factor depending on the number parity π_N is chosen so the OES centered on even and odd neutron number N will both be positive. An analogous proton OES indicator $\Delta^{(3)}(Z)$ is obtained by fixing the neutron number N and replacing N by Z in Eq. (14). The impact of time-odd mean fields on this quantity has been discussed in detail in Ref. [26].

In order to extract the ground state in the odd-mass nucleus, the binding energies are calculated for a number of the 1-qp configurations based on the orbitals active in the vicinity of the Fermi level and then the lowest in energy state is assigned to the ground state. Such calculations are very complicated and time-consuming. As a result, they were done only in a few cases (see Ref. [41] and references therein) on the H(F)B level of the DFT framework. To our knowledge, the detailed analysis of the $\Delta^{(3)}$ indicators has not been performed so far in the RHB framework because of the complexity of the definition of the ground states in odd-mass nuclei. Thus, this manuscript represents a first attempt of the systematic analysis of pairing correlations via fully self-consistent calculations of the $\Delta^{(3)}$ indicators in the RHB framework.

The $\Delta^{(3)}$ indicators are analyzed in the CRHB and CRHB + LN frameworks. There are several reasons for a such comparative study. First, the HFB [RHB] calculations without approximate particle number projection by means of the LN method are still used in the study of rotational bands [75,76], one-quasiparticle states [41], fission barriers [33,76], and fission half-lives [77] of actinides and superheavy nuclei in the methods which employ the Brink-Booker part of finite-range Gogny force in the pairing channel. Second, the calculations with the LN method are more time-consuming and frequently less numerically stable than the ones without it. As a consequence, it is important to understand the similarities and differences between the CRHB and CRHB + LN results related to pairing.

The CRHB calculations were performed with original strength of the Brink-Booker part of the Gogny D1S force

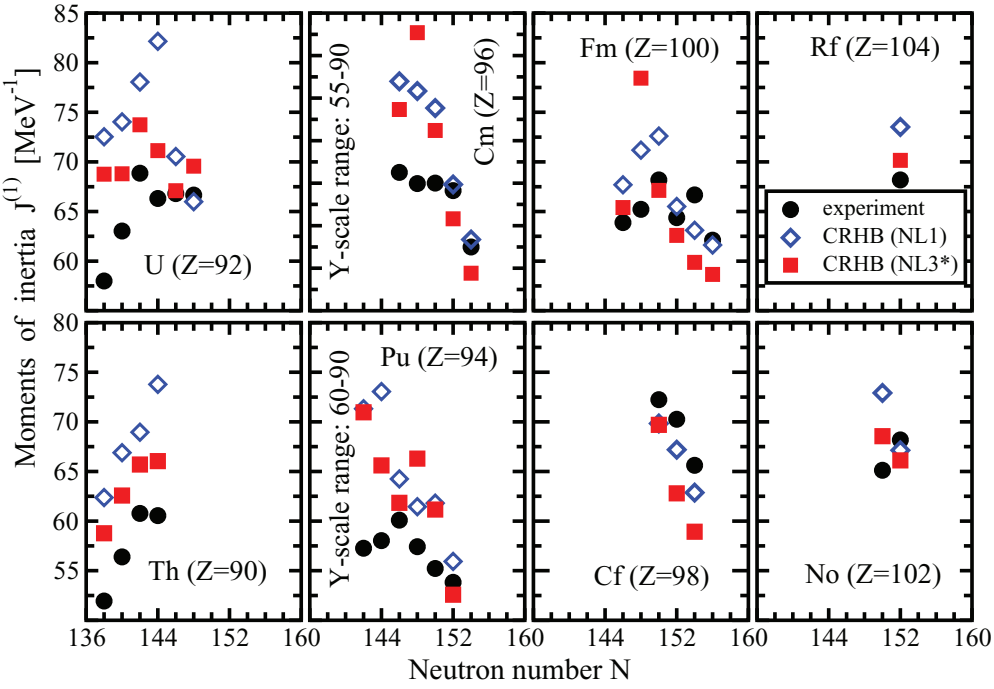

FIG. 4. (Color online) The same as in Fig. 2 but for the CRHB calculations with scaling factor $f = 1.0$ and only for the nuclei in which experimental data are available. To make the comparison with Fig. 2 easier, the difference between the highest and lowest values on the vertical axis is kept the same as in Fig. 2; the only exception is the panel with the Cm isotopes. As a consequence, the different ranges for vertical axis are used for top and bottom panels. Moreover, the different ranges are used for vertical axis in the case of the Cm and Pu isotopes.

(scaling factor $f = 1.0$), which, according to Ref. [1], provides good description of the moments of inertia in ^{254}No over experimentally measured spin range. These calculations also reasonably well describe the moments of inertia at low spin (Fig. 4). Systematic nonrelativistic investigations within cranked HFB approach based on a Gogny D1S force also give a reasonable description of the moments of inertia in actinides [75,76,78]. For example, the results obtained in Ref. [78] are close to the CRHB(NL3*) ones. Considering the similarities of these two approaches (CRHB and Gogny HFB) [40], this is not surprising.

Figures 5–8 show the $\Delta^{(3)}$ indicators obtained in the CRHB calculations using the results of the calculations of odd-mass nuclei of Ref. [41]. In average, they are close to experimental data. For the proton subsystem, the rms deviations from experimental $\Delta_{\nu}^{(3)}$ indicators are 0.22 and 0.15 MeV in the CRHB calculations with the NL1 and NL3* parametrizations, respectively. For the neutron subsystem, these deviations are 0.10 and 0.125 MeV, respectively. This compares favorably with global fits of pairings to the $\Delta^{(3)}$ indicators in the Skyrme DFT calculations of Refs. [38,39] in which an rms accuracy of about 0.25 MeV has been obtained for $\Delta^{(3)}$.

The inclusion of the LN method into the calculations leads to a decrease of the scaling factor by approximately 10% [to $f_{\rm av} = 0.9147$ and $f_{\rm av} = 0.899$ in the NL1 and NL3* parametrizations, respectively (see Sec. III B)]. The experimental moments of inertia at low spin are described rather well with these scaling factors; see the discussion in Sec. III C. Figures 5 and 6 show the $\Delta^{(3)}$ indicators calculated in the CRHB + LN approach. However, the convergence problems in the calculations of one-quasiparticle states in odd-mass nuclei, emerging from the interaction of the blocked orbital with others, appear more frequently when approximate particle number projection by means of the Lipkin-Nogami method is employed. This is most likely due to additional nonlinearities of the LN method. Note that such convergence problems are typical for the methods employing iterative diagonalization schemes for the solution of the mean-field equations and appear both in the CRHB and CRHB + LN calculations. As a consequence, it was not possible to obtain the $\Delta^{(3)}$ indicators in the CRHB + LN calculations in a significant number of the cases since no reliable definition of the ground state in some odd-mass nucleus is possible. This is despite the fact that the CRHB + LN calculations of low-energy spectra in odd-mass nuclei were restricted to the three lowest-energy one-quasiparticle configurations obtained in the CRHB calculations of Ref. [41]. Such a simplified procedure (as compared with the one used in the CRHB calculations of Ref. [41]) can be used since the quasiparticle spectra calculated within CRHB [with original ($f = 1.0$) strength of the Brink-Booker part of the Gogny D1S force] and CRHB + LN (with attenuated strength of the Brink-Booker part) are very similar; the difference in the energies of three lowest-energy one-quasiparticle configurations is typically less than 100 keV and the configuration ordering is the same (see, for example, Fig. 23 in Ref. [1]). However, the lack of convergence in either of these three configurations disqualifies an odd-mass nucleus from consideration for the calculations of the $\Delta^{(3)}$ indicator.

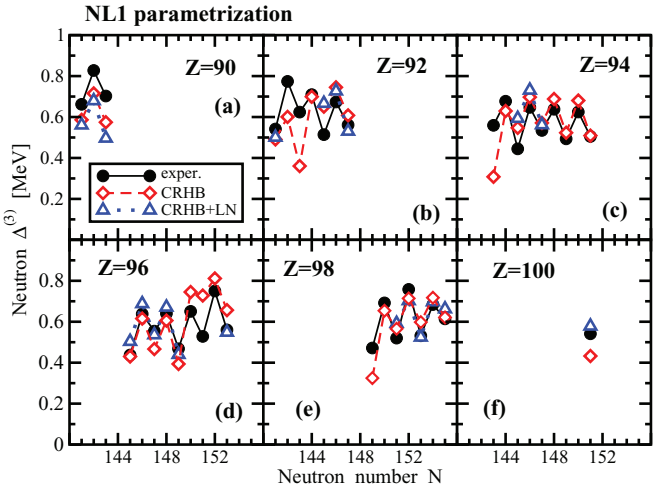

FIG. 5. (Color online) Experimental and calculated neutron three-point indicators $\Delta_\nu^{(3)}(N)$ as a function of neutron number N. The results of the CRHB and CRHB + LN calculations with the NL1 parametrization are shown.

Because of these convergence problems and the time-consuming nature of the CRHB + LN calculations for one-quasiparticle configurations, the systematic analysis of the $\Delta^{(3)}$ indicators shown in Figs. 5 and 6 has been performed only for the NL1 parametrization. The CRHB + LN calculations rather well describe these observables; the rms deviations from experiment are 0.11 and 0.084 MeV for proton and neutron subsystems, respectively. For the same (as in CRHB + LN calculations) set of nuclei, these deviations are 0.18 and 0.077 MeV in the CRHB calculations. As a result, for the neutron subsystem the results of both calculations are similar, while proton $\Delta^{(3)}$ indicators are better described in the CRHB + LN calculations. The fit of the strength of the pairing force to experimental moments of inertia (see Sec. III C) and the fact that the LN method leads to a better (on average) description of the $\Delta^{(3)}$ indicators [38] may be responsible for observed differences in the CRHB + LN and CRHB results.

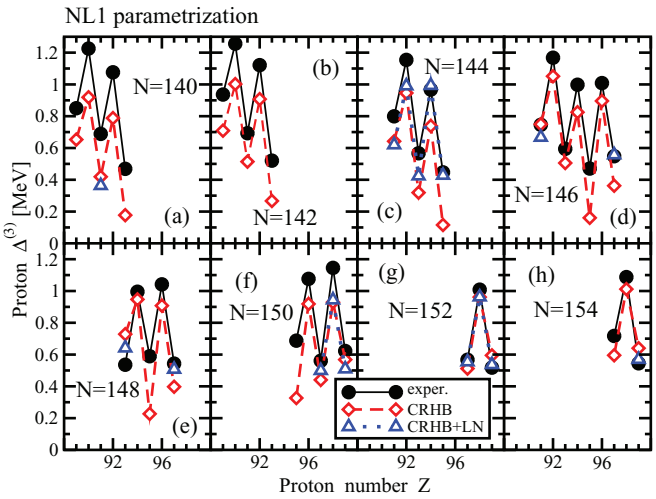

FIG. 6. (Color online) The same as in Fig. 5 but for proton three-point indicators $\Delta_\pi^{(3)}(Z)$ as a function of proton number Z.

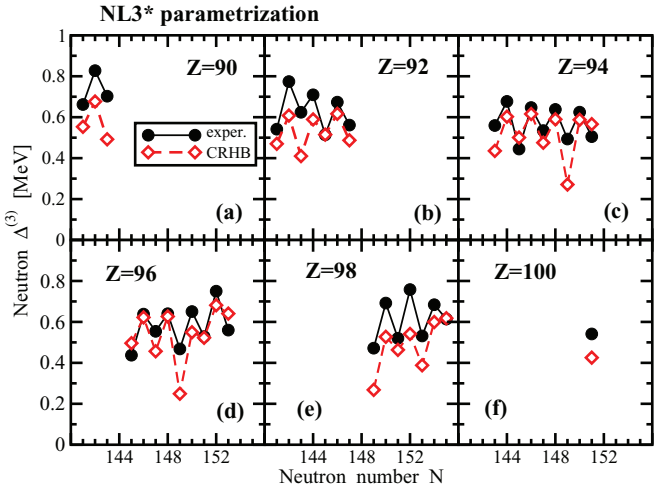

FIG. 7. (Color online) The same as in Fig. 5 but for the NL3* parametrization. Theoretical values have been obtained within the CRHB framework.

The comparison of calculated moments of inertia, three-point indicators $\Delta^{(3)}$, and individual scaling factors f_i allows us to make a number of important conclusions. First, there is a strong correlation between the definitions of pairing strengths by means of the moments of inertia and three-point indicators. For example, the calculations for both of these physical observables show that pairing has to be slightly stronger at low values of neutron number N. The definitions of pairing strength via these two observables are complimentary. This is because (i) it is difficult to disentangle proton and neutron contributions to pairing when considering the moments of inertia and (ii) the $\Delta^{(3)}$ indicators are affected by particle-vibration coupling and depend on correct reproduction of the ground states in odd-mass nuclei (see Sec. III E for details).

Second, approximate particle number projection by means of the LN method is important for a better description of particle-number dependencies of the moments of inertia.

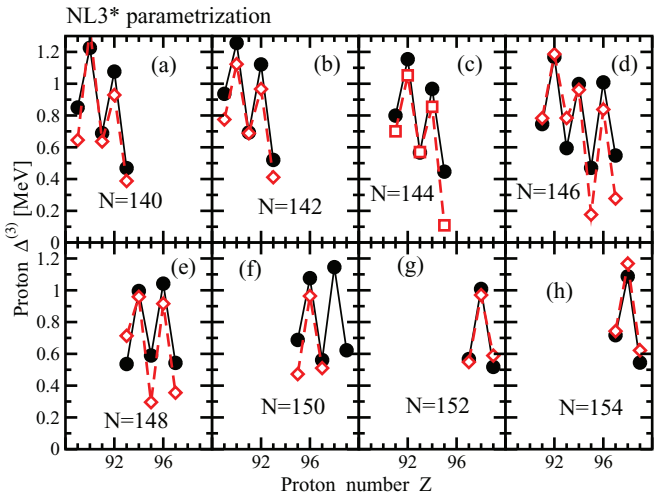

FIG. 8. (Color online) The same as in Fig. 6 but for the NL3* parametrization. Theoretical values have been obtained within the CRHB framework.

Although the average description of the moments of inertia in the CRHB calculations seen in Fig. 4 can be improved by an increase of the strength of pairing by few percentages, this increase will not resolve wrong particle-number dependencies for calculated $J^{(1)}$ and will not lead to the same level of accuracy of the description of $J^{(1)}$ as seen in the CRHB + LN calculations (Fig. 2).

Third, obtained results clearly show that the strength of pairing in the CRHB calculations has to be by 10–15% larger than the one in the CRHB + LN calculations in order to reproduce the experimental observables sensitive to pairing with comparable level of accuracy. This clarifies the problem with different pairing strengths employed previously in the CRHB and CRHB + LN approaches which was discussed in the introduction. Considering the weak dependence of the results of the CDFT parametrization, the results presented in the current manuscript and the ones obtained in Refs. [14,40] suggest that the scaling factors f of the Brink-Booker part of the Gogny D1S force ∼0.9 and ∼1.0 (∼1.0 and ∼1.1) have to be used in the actinides and rare-earth/lighter nuclei in the CRHB + LN (CRHB) calculations, respectively. Although this weak dependence on the CDFT parametrization has been verified here only for the NL1 and NL3* parametrizations, we believe that it will hold also for other modern CDFT parametrizations. The pairing properties depend on single-particle level densities which in turn are defined by the Lorentz effective mass $m*(k_F)/m$ of nucleons at the Fermi surface. However, these effective masses are very similar for all successful CDFT parametrizations [41,45,46,56,58,61,62].

E. The sources of the deviations between theory and experiment for the $\Delta^{(3)}$ indicators

The accuracy of the description of the $\Delta^{(3)}$ indicators depend on a number of factors, some of which were investigated in Refs. [38,39,74]. Here, we will briefly discuss two factors which have been ignored (and even not mentioned) in the absolute majority of the studies of pairing based on odd-even staggerings of binding energies. These are the correctness of the reproduction of the ground states in odd-mass nuclei and the impact of particle-vibration coupling (PVC). They clearly affect the $\Delta^{(3)}$ indicators and limit the accuracy with which the experimental data can be described in model calculations.

The structure of the ground state in odd-mass nucleus is not always correctly reproduced in model calculations and this can have an impact on the calculated $\Delta^{(3)}$ value. Indeed, the calculations within the RHB theory with the NL1 and NL3* parametrizations [41], the Hartree-Fock + BCS approach with different parametrizations of the Skyrme forces [79] as well as the FRDM model employing phenomenological folded-Yukawa potential [79] show that only approximately 40% of the ground states in odd-mass deformed nuclei are correctly reproduced.

However, different single-particle states have different polarization effects for quadrupole and hexadecapole moments (this is clearly seen in the statistical analysis presented in Fig. 4 of Ref. [41]) and for time-odd mean fields (see Table IV in Ref. [1]). These polarization effects will impact the binding energies of odd-mass nuclei. If the structure of calculated ground state differs from experimental one, the difference in polarization effects of these two states contributes into the discrepancy between calculated and experimental $\Delta^{(3)}$ values. This effect is expected to be minimal (maximal) when these two states have similar (significantly different) deformation-driving properties. The analysis of a number of the cases suggests that the wrong ground state in an odd-mass nucleus can sometimes modify the $\Delta^{(3)}$ indicator by as much as 150 keV.

Additional binding due to time-odd mean fields in odd-mass nuclei is rather small in actinides and shows weak dependence on the blocked orbital (see Ref. [26] and Table IV in Ref. [1]). Thus, even if the ground state in an odd-mass nucleus is wrong in model calculations, the difference in polarization effects due to time-odd mean fields of the wrong and correct states will only marginally (by less than 20–30 keV) affect the $\Delta^{(3)}$ indicators.

It is well known from the studies of spherical odd-mass nuclei that particle-vibration coupling affects the binding energies (see Refs. [25,80]). So far, no similar studies are available in deformed nuclei in the PVC models based on relativistic or nonrelativistic DFT because of the complexity of the problem. However, the calculations within the quasiparticle-phonon model based on phenomenological Woods-Saxon potential indicate that the lowest states of odd-mass actinides have mainly quasiparticle nature [81,82] and that the corrections to their energies due to PVC are typically less than 150 keV [83]. These corrections will definitely have an impact on the $\Delta^{(3)}$ indicators.

These two effects can be a source of the deviations between theory and experiment seen in Figs. 5–8. However, the fact that, on average, the moments of inertia and the $\Delta^{(3)}$ indicators are reasonably well described (especially in the CRHB + LN calculations) with the same strength of pairing suggests that, apart from some combinations of proton and neutron numbers, these two effects do not contribute significantly. Note that the moments of inertia of even-even nuclei are significantly less affected by these two effects. Therefore, in some sense they are a more robust measure of pairing correlations.

IV. ROTATIONAL PROPERTIES OF EVEN-EVEN NUCLEI

Figures 9 and 10 show the results of systematic calculations for the kinematic moments of inertia of the ground-state rotational bands in even-even actinides. Either a sharp or more gradual increase of the kinematic moments of inertia is observed at $\Omega_x \approx 0.2$–0.30 MeV. Figure 11 shows the proton and neutron contributions to the kinematic moments of inertia. These increases in $J^{(1)}$ are due to the alignments of the neutron $j_{15/2}$ and proton $i_{13/2}$ orbitals, which in many cases take place at similar rotational frequencies (see Fig. 11). It is clear that the situation in actinides is more complicated than in the rare-earth region in which the $h_{11/2}$ protons align substantially later than the $i_{13/2}$ neutrons. This simultaneous alignment of proton and neutron orbitals is also present in a number of theoretical models discussed below.

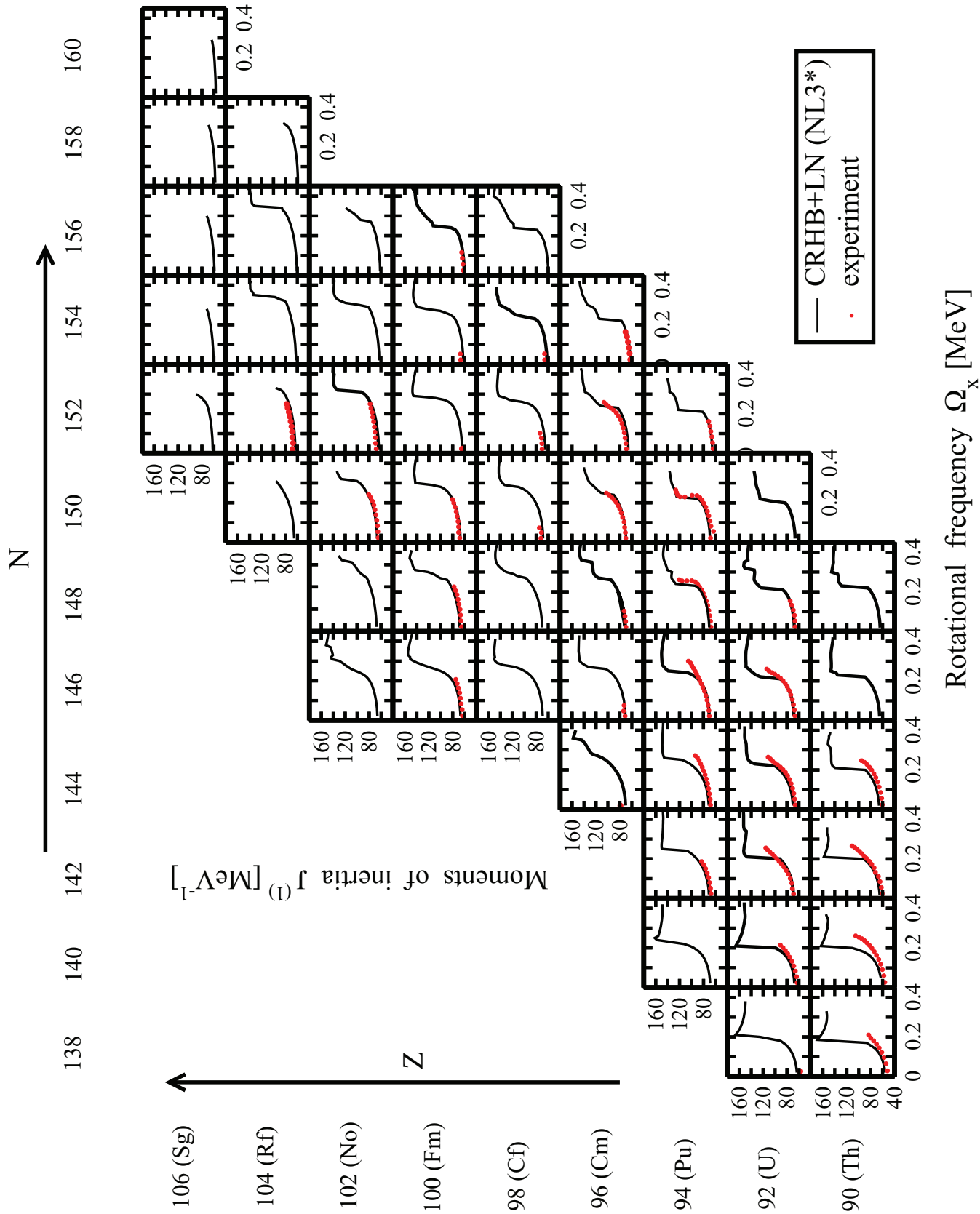

FIG. 9. (Color online) The experimental and calculated moments of inertia $J^{(1)}$ as a function of rotational frequency Ω_x. The calculations are performed with the NL3* parametrization of CDFT. Calculated results and experimental data are shown by black lines and red small solid circles, respectively. Although some calculations suggest that ^{228}Th is octupole soft (see Fig. 7 in Ref. [42]), its moment of inertia is rather well described in our calculations with no octupole deformation.

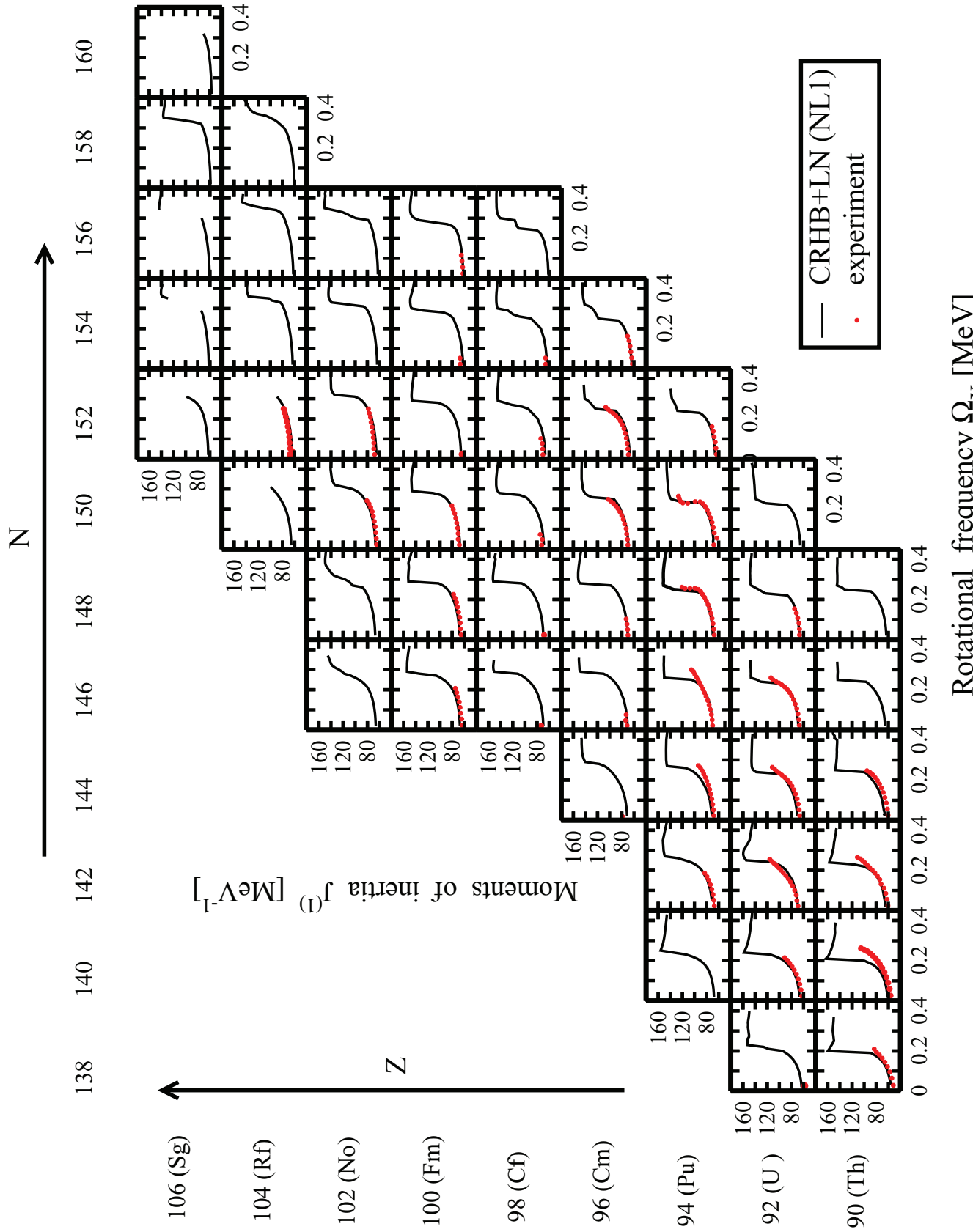

FIG. 10. (Color online) The same as in Fig. 9 but for the calculations with the NL1 parametrization.

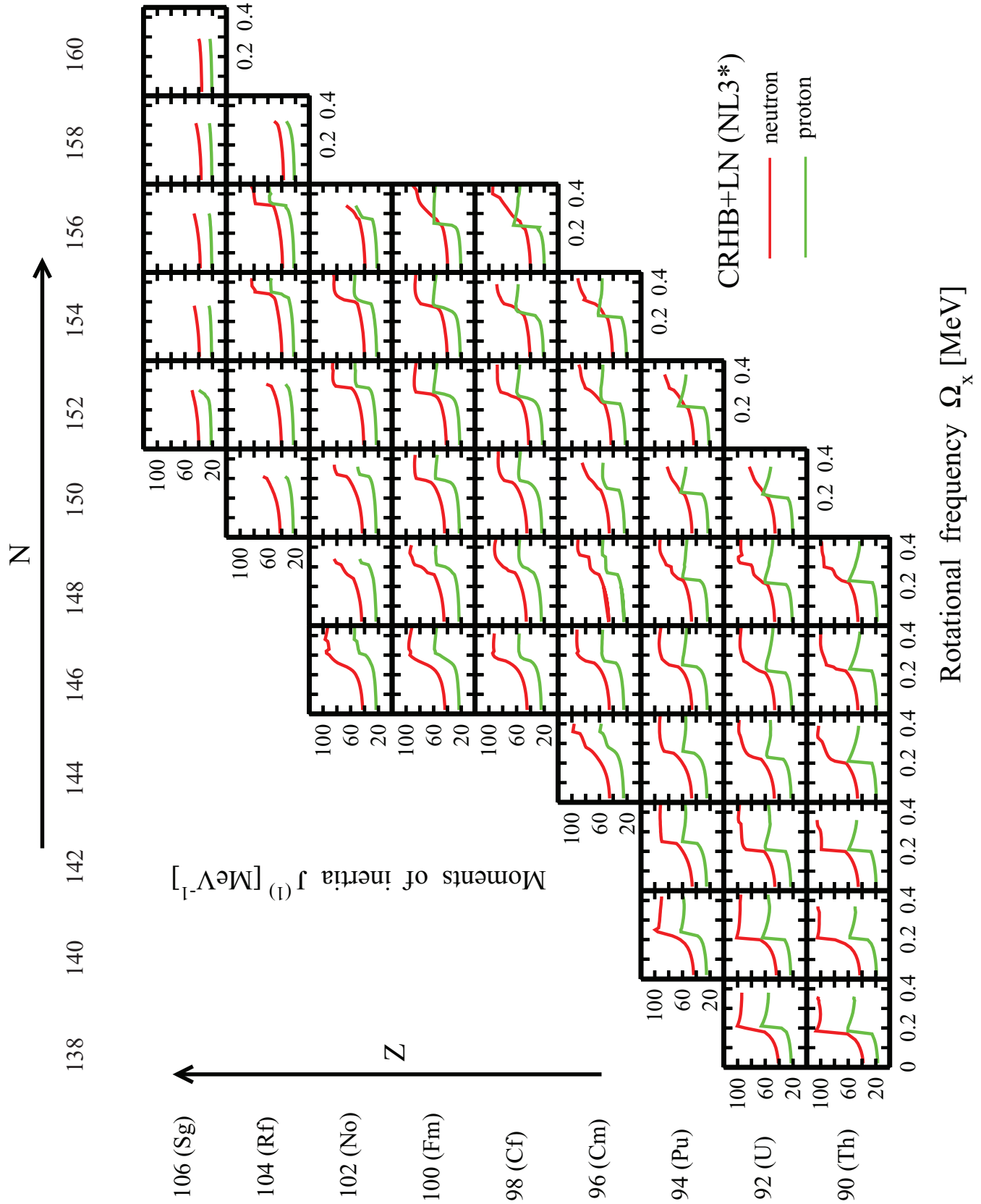

FIG. 11. (Color online) Calculated proton and neutron contributions to kinematic moments of inertia $J^{(1)}$ as a function of rotational frequency Ω_x. The calculations are performed with the NL3* parametrization of CDFT.

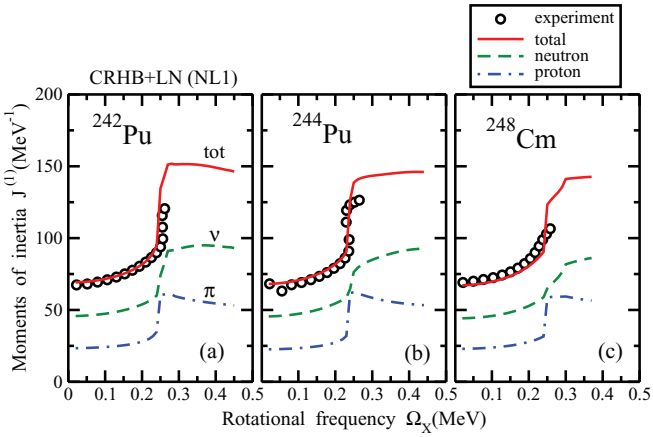

FIG. 12. (Color online) The experimental and calculated kinematic moments of inertia $J^{(1)}$ of ground-state rotational bands in ^{242,244}Pu and ^{248}Cm as a function of rotational frequency Ω_x. The calculations are performed with the NL1 parametrization.

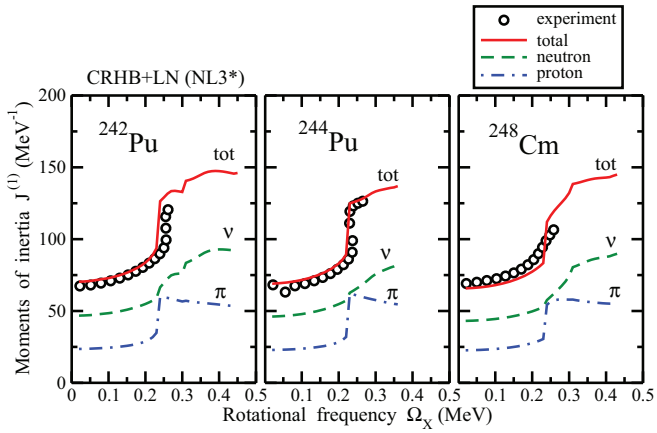

FIG. 13. (Color online) The same as in Fig. 12 but for the results obtained with the NL3* parametrization.

One can see that the CRHB + LN calculations rather well describe the experimental kinematic moments of inertia and their evolution with rotational frequency. The results obtained with the NL1 and NL3* parametrizations are rather similar in the majority of the cases (compare Figs. 9 and 10). Only in the ^{238,240}Pu, ^{236,238}U, and ^{230,232}Th nuclei. The CRHB + LN(NL1) calculations predict a sharp upbending in $J^{(1)}$ at $\Omega_x \sim 0.2$ MeV which is not present in the experimental data. The same problem exists also in the CRHB + LN(NL3*) calculations, but in addition to the above-mentioned set of nuclei an earlier alignment (as compared with experiment) also is seen in the calculations for the ^{234}U and ^{234}Th nuclei. This indicates that the calculated details of the band crossings depend more on the CDFT parametrization than the kinematic moments of inertia before band crossings.

A number of theoretical calculations based on the cranking model discussed below also do not reproduce the rotational properties of these nuclei at the highest spins. This suggests that some effect not included in the model framework plays a role at the spins at which sharp band crossing take place in model calculations. As discussed below, the stabilization of octupole deformation at high spin is most likely a candidate for this effect.

So far, the observation of a sharp upbending has been reported only in ^{242,244}Pu.[2] Figures 12 and 13 compare experimental data with model calculations. The backbending is complete in ^{244}Pu and the CRHB + LN(NL3*) calculations rather well describe it [Fig. 13(b)]; the sharp alignment of the proton $i_{13/2}$ orbitals is a source of this backbending and the neutron $j_{15/2}$ alignment proceeds gradually over an extended frequency range. On the contrary, sharp alignments of the proton and neutron pairs take place at the same frequency in the CRHB + LN(NL1) calculations [Fig. 12(b)] and they somewhat overestimate the kinematic moment of inertia above the band crossing. The same situation with the alignments of the proton $i_{13/2}$ and neutron $j_{15/2}$ pairs exists also in the CRHB + LN(NL1) and CRHB + LN(NL3*) calculations for ^{242}Pu. They accurately reproduce the evolution of kinematic moments of inertia with frequency and the frequency of the paired band crossing [Figs. 12(a) and 13(a)]. However, since upbending is not complete in experiment it is impossible to judge whether the simultaneous sharp alignments of proton and neutron pairs really take place in nature. Smooth upbending takes place in ^{248}Cm [Fig. 12(c)]. The CRHB + LN(NL1) [Fig. 12(c)] and CRHB + LN(NL3*) [Fig. 13(c)] calculations suggests that this upbending is predominantly due to the proton $i_{13/2}$ alignment. However, the interaction between the g and S bands in the band crossing region is too weak in the proton subsystem, which leads to sharp upbending in model calculations.

The calculated kinematic moments of inertia at the frequencies below and above band crossing only weakly depend on the CDFT parametrization (compare Figs. 9 and 10). On the contrary, the rate of the increase of the kinematic moment of inertia in the band crossing region of respective subsystem (proton or neutron) depends more sensitively on employed parametrization. Proton and neutron contributions to the kinematic moments of inertia obtained in the CRHB + LN(NL3*) calculations are shown in Fig. 11. In the CRHB + LN(NL1) calculations, the alignments of the proton and neutron pairs are similar to the ones of the CRHB + LN(NL3*) calculations in the majority of the cases; this is a reason why no figure similar to Fig. 11 is presented for the CRHB + LN(NL1) results. The largest dependence on the parametrization is seen in the calculated alignments of the neutron $j_{15/2}$ pairs for which the increase of the neutron $J^{(1)}$ values in the band crossing region is either sharper or more gradual in the CRHB + LN(NL1) calculations as compared with the CRHB + LN(NL3*) ones in ^{236,238}Th, ^{238,240,242}U, ^{236,240,242,244}Pu, ^{240,244}Cm, ^{246,254}Cf, ^{248,256}Fm, and ^{258}No. On the contrary, such differences are seen in proton subsystem only in ^{240,244}Cm, ^{246}Cf, and ^{246,248}Fm. These differences between the CRHB + LN(NL3*)

[2]Similar sharp upbendings have also been observed in ground-state rotational bands of ^{246,250}Cm and ^{250}Cf [84]. Their properties are well described in the CRHB + LN calculations with the NL1 and NL3* parametrizations.

and CRHB + LN(NL1) results are in part due to the differences in the single-particle structure obtained in the NL1 and NL3* parametrizations [41].

Rotational properties of actinides have been in the focus of extensive studies within the cranked shell model (CSM) [7,8,85–87], the rotating shell model [89], and the cranked Hartree-Fock-Bogolibov (CHFB) [6,88] approach based on the phenomenological potentials (Woods-Saxon [6,87] and Nilsson [7,8,86,89]) or quadrupole-quadrupole force Hamiltonian [85,88]). Similar to our calculations, the simultaneous or near-simultaneous alignments of neutron $j_{15/2}$ and proton $i_{13/2}$ orbitals define rotational and band crossing properties. However, these calculations suffer from a number of simplifications such as fixed deformations [8,86–89], reduced or/and fixed pairing gaps [87,89], the absence of particle number projection [85,87,88], the restriction to axial symmetry [6–8,86] or extensive local fit of model parameters to experimental data [8,89]. The cranked HFB calculations based on the Gogny D1S force [75,76] have also been performed without particle number projection. Such simplifications are avoided in the current CRHB + LN calculations.

Let illustrate a typical situation by an example of extensive cranking calculations employing the universal parametrization of the Woods-Saxon (WS) potential [87]. In these calculations, for each nucleus the deformation was fixed at the value calculated for the ground state. It was found that the pairing gaps equal to 80% of the value defined from five-point odd-even mass difference have to be used to better explain observed properties. However, required quenching of pairing gap has not been explained. The alignments of neutron $j_{15/2}$ and proton $i_{13/2}$ orbitals define rotational and band crossing properties. However, there is no consistent explanation for the absence of experimental neutron $j_{15/2}$ band crossings in a number of nuclei. It was also concluded that based on available data it is difficult to determine how accurately the WS calculations predict the crossing frequencies and interaction strengths.

While the CRHB + LN calculations well describe the sharp $i_{13/2}$ proton alignment observed in the rotational sequences of the $^{242-244}$Pu nuclei (see Sec. V B for ^{243}Pu results), they fail to reproduce the absence of such alignments in ^{238,240}Pu, ^{234,236,238}U, and ^{230,232,234}Th (see Figs. 10 and 9). Such problem exists in all cranking calculations; see references cited above in this section for details. Although the cranking calculations may not be completely adequate for the band crossing region [90], a reasonable description of band crossings in $^{242-244}$Pu suggests that this is not main source of the deviations between theory and experiment.

It is quite likely that this problem is related to the stabilization of octupole deformation at high spin which is not taken into account in model calculations. Stable octupole deformation has been shown to delay alignment processes [91] and this may explain the differences between theory and experiment. Indeed, the analysis of the spectra of the ground-state positive-parity and lowest-negative-parity bands of ^{232}Th, ^{238}U, and ^{240}Pu indicates a second-order phase transition from reflection-symmetric to reflection-asymmetric shapes in these bands (Ref. [92]). This phase transition takes place at spins $I \approx 12$–$15\hbar$. This analysis is based on the mathematical techniques of supersymmetric quantum mechanics, a two-center octupole wave-function ansatz, and the Landau theory of phase transitions.

It was also suggested that strong octupole correlations in rotational bands of some actinides may be interpreted as the rotation-induced condensation of octupole phonons having their angular momentum aligned with the rotational axis [93]. When the rotation of the condensate and the quadrupole shape of the nucleus synchronize, the collective motion becomes the familiar rotation of a static octupole shape. The experimental data on ^{238,240}Pu [94] agrees with such an interpretation and the experimental data in ^{238}U show the indications of this process [95]. Indeed, at the highest spins the yrast and the octupole bands in ^{238,240}Pu appear to merge into a single sequence of levels with alternating spin and parity, and large intrinsic dipole moments were inferred from the measured $B(E1)/B(E2)$ ratios [94]. In addition, there are indications of the formation of parity doublets at high spin in ^{239}Pu [96]. All that suggests the stabilization of octupole deformation at the highest spins in these nuclei. Furthermore, the systematics of the lowered energies of the 1^- states and the lowered hindrance factors in α decay populating these 1^- states suggest an increased octupole correlations for Pu and U nuclei with 144 and 146 neutrons [97].

New experimental data on ^{230}Th shows the signatures of the stabilization of octupole deformation [98]. On the other hand, the extension of ground state and especially octupole vibrational rotational bands up to higher spin is needed in order to see whether this is also a case in ^{234,236}U and ^{232,234}Th nuclei.

In the context of the study of rotational properties of actinides, it is interesting to mention that the same $j_{15/2}$ neutron and $i_{13/2}$ orbitals lie at the Fermi surface in the superdeformed nuclei of the $A \sim 190$ mass region. Remarkably, most superdeformed nuclei of this region exhibit a surprisingly smooth and gradual increase of their moments of inertia with frequency emerging from the alignment of these orbitals and this process is very well described in the CRHB + LN(NL1) calculations [13].

V. ROTATIONAL PROPERTIES OF ODD-MASS NUCLEI

Rotational properties of one-quasiparticle configurations provide important information on the impact of odd particle/hole on alignment and pairing properties. They can also provide an additional constraint on the structure of single-particle states, which is especially important for the light superheavy nuclei at the edge of the region where spectroscopic studies are still feasible (the nuclei with masses $A \sim 255$ and proton number $Z \geqslant 102$). This is because alternative methods of configuration assignment either provide the results with a low level of confidence or are not possible [3]. Unfortunately, our knowledge of the accuracy of the description of rotational properties of one-quasiparticle configurations in the DFT frameworks is extremely limited since no systematic investigation of such properties has been

performed so far. Across the nuclear chart they were studied only in ^{251}Md [3], ^{241}Am [3], ^{253}No [66], and ^{255}Lr [67] within the CRHB + LN approach, in ^{253}No [20,21,66], ^{255}No, ^{251}Md, and ^{255}Lr [21], as well as in superdeformed rotational bands of ^{193}Pb and ^{193}Hg [100] in the cranked HFB approach based on Skyrme forces. To our knowledge, such studies have not been performed in the cranked HFB approach based on the Gogny forces. It is also surprising that no systematic investigation of rotational structures in odd-mass actinides is available in the MM approach; the occasional cranked shell model calculations characterized by a number of parameters adjusted to experimental data should not be considered as a replacement for full-fledged MM calculations. In order to fill this gap in our knowledge, a systematic investigation of rotational properties of odd-mass actinides is performed. Even with present computational facilities, it is still a nontrivial problem because of three reasons discussed below.

First, a proper description of odd nuclei implies the loss of time-reversal symmetry of the mean field, which is broken both by the unpaired nucleon [26] and by the rotation [28]. As a consequence, time-odd mean fields and nucleonic currents, which cause the *nuclear magnetism* [43] have to be taken into account.

Second, the effects of blocking due to odd particles have to be included in a fully self-consistent way. This is done in the CRHB + LN code according to Refs. [101–103]. The blocked orbital can be specified by different fingerprints such as the dominant main oscillator quantum number N of the wave function, the dominant Ω quantum number (Ω is the projection of the angular momentum on the symmetry axis) of the wave function, the particle or hole nature of the blocked orbital, the position of the state within specific parity/signature/dominant N/dominant Ω block, or their combination. For a given configuration, possible combinations of the blocked orbital fingerprints were defined from the analysis of calculated quasiparticle spectra in neighboring even-even nuclei and the occupation probabilities of the single-particle orbitals of interest in these nuclei.

Third, variational solutions with blocked orbital(s) are numerically less stable than the ones for the ground-state bands in even-even nuclei. This is because, at each iteration of the variational procedure, the blocked orbital has to be properly identified. This identification is complicated by the fact that Ω is not a conserved quantum number in the CRHB + LN code. As a consequence, closely lying orbitals within a given parity/signature block can interact and exchange a character. The convergence problems, emerging from the interaction of the blocked orbital with others, appear quite frequently. The interaction strength of these orbitals is one ingredient affecting the convergence. Another is the relative energies of interacting orbitals. Different CDFT parametrizations are characterized by different single-particle specta [1] (see also Nilsson diagrams presented in Fig. 15). As a result, the convergence problems for specific blocked solution can show up in one parametrization but will not affect the solution in another parametrization. The structure of wave function of blocked orbital and the energy of this orbital with respect to other orbitals change as a function of rotational frequency. While converging in some frequency range the solution for a given blocked orbital may face the convergence problems outside this range. The convergence also depends on the initial conditions; for some configurations the solution at given frequency converges if we start from self-consistent solution of the neighboring frequency point but does not converge if we start from the fields generated by the Woods-Saxon potential and diagonal Δ matrix. This feature has been used in the calculations. The employed combination of blocked orbital fingerprints also affects the numerical convergence; the solution can converge for one combination but face the convergence problems for another one. Thus, for a number of configurations several combinations of blocked orbital fingerprints have been used.

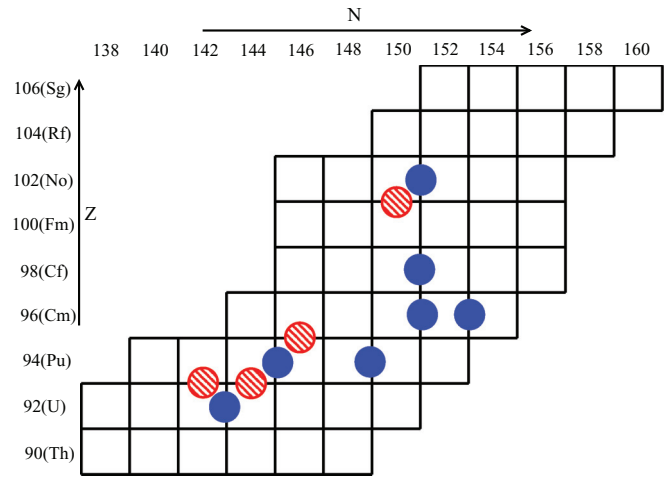

FIG. 14. (Color online) The chart of nuclei investigated in the current work. Solid blue and red shaded circles indicate studied odd-neutron and odd-proton nuclei, respectively. The nucleus has $Z + 1$ protons and N neutrons if its circle is located between the (Z, N) and $(Z + 2, N)$ boxes. Alternatively, it has Z protons and $N + 1$ neutrons if its circle is located between the (Z, N) and $(Z, N + 2)$ boxes.

The results of systematic calculations are presented in Figs. 16 and 18–27. All odd-mass nuclei with long rotational sequences are considered in this investigation; the only exception is the ^{255}Lr nucleus since the configuration assignment for observed rotational structure is still under debate [67]. These nuclei are shown by circles in Fig. 14. Other odd-mass nuclei, the rotational sequences of which contain only few low-spin states, are ignored in this investigation since we are interested in the evolution of rotational properties with spin.

Figure 15 shows the Nilsson diagrams obtained for ^{244}Cm in the calculations with the NL1 and NL3* parametrizations. This nucleus is located in the center of the region of odd-mass nuclei under study (Fig. 14). The single-particle orbitals which can be observed in odd-mass nuclei of the region under study are labeled by the Nilsson labels. Moreover, long rotational sequences built on some of these orbitals have been experimentally observed (see discussion in Secs. V A and V B). Although the general structure of the Nilsson diagrams is the same in the NL1 and NL3* parametrizations, the relative energies of different single-particle orbitals and their energies

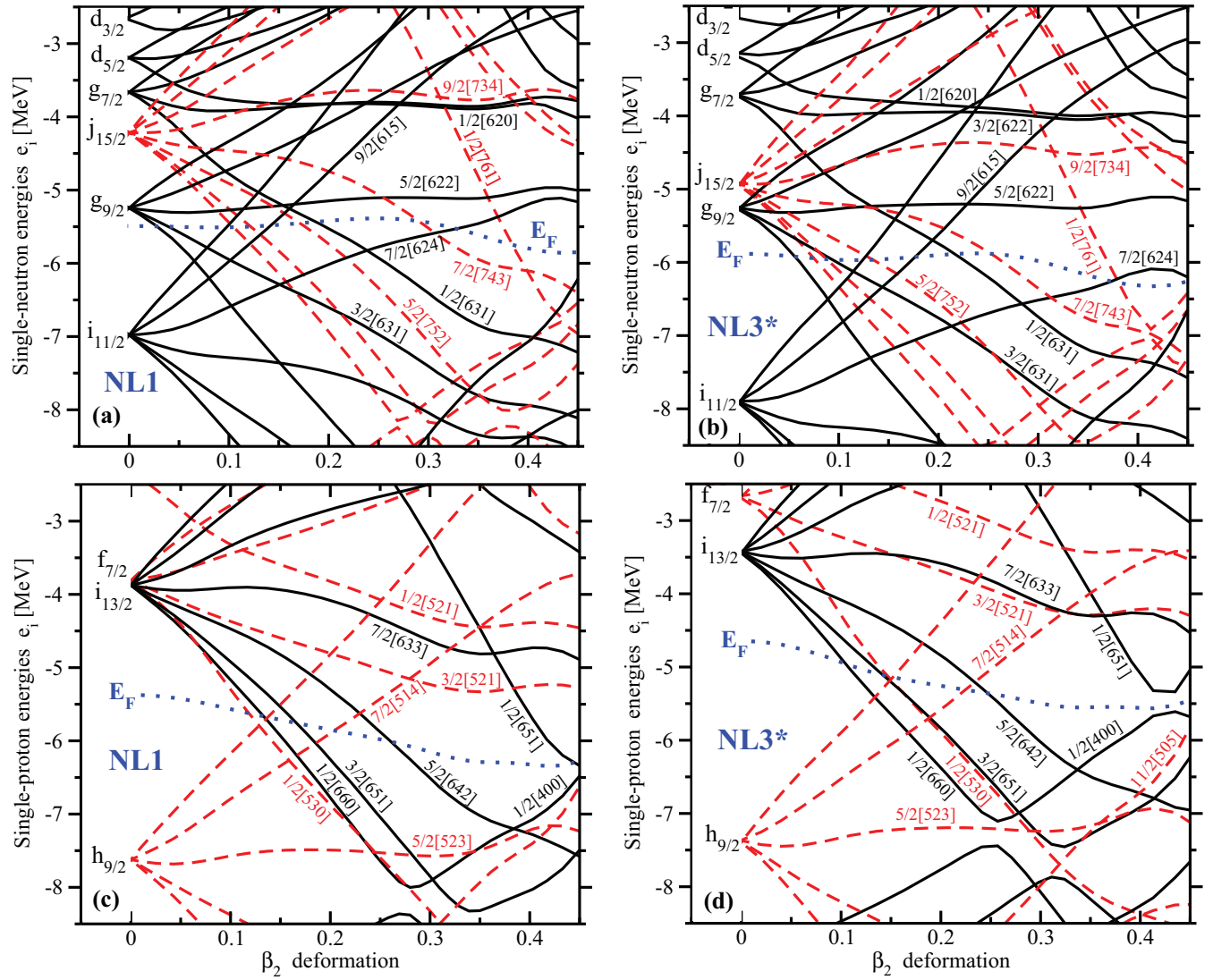

FIG. 15. (Color online) Proton and neutron single-particle energies in ^{244}Cm as a function of quadrupole deformation β_2 obtained in the calculations with the NL1 and NL3* parametrizations. Solid black and red dashed lines are used for positive- and negative-parity states, respectively. The energy of the Fermi level is shown by the blue dotted line. Deformed single-particle orbitals of interest are labeled by the Nilsson quantum numbers $\Omega[Nn_z\Lambda]$.

with respect to the Fermi level at the deformation $\beta_2 \sim 0.3$ typical for nuclei under study (see Fig. 3) depend strongly on parametrization. For example, the $\pi 3/2[521]$ and $\pi 7/2[633]$ orbitals are nearly degenerate in the NL3* parametrization [Fig. 15(d)]. However, they are separated by 0.5 MeV gap in the NL1 parametrization [Fig. 15(c)]. Such differences in the energies of deformed states can be traced back to the differences in the single-particle energies at the spherical shape [1].

We compare experimental and calculated kinematic moments of inertia $J^{(1)}$ of one-quasiparticle configurations in odd-mass nuclei and ground-state rotational band in the reference even-even mass nucleus. Figure 16 is an example of such a comparison and the figures for other nuclei follow its pattern. Two parametrizations, namely NL1 and NL3*, are used in the calculations in order to see how the results depend on the parametrization. We drop the panel with specific parametrization when it was not possible to obtain the converged solution for it. The calculations were attempted for all experimentally observed configurations of odd-mass nuclei indicated in Fig. 14; the absence of calculated curve for specific configuration indicates that no convergence has been obtained for it.

A. Odd-proton nuclei

Long rotational bands based on different single-particle orbitals have been observed in odd-proton ^{241}Am, ^{235,237}Np, and ^{251}Md nuclei. We discuss them below separately, nucleus by nucleus.

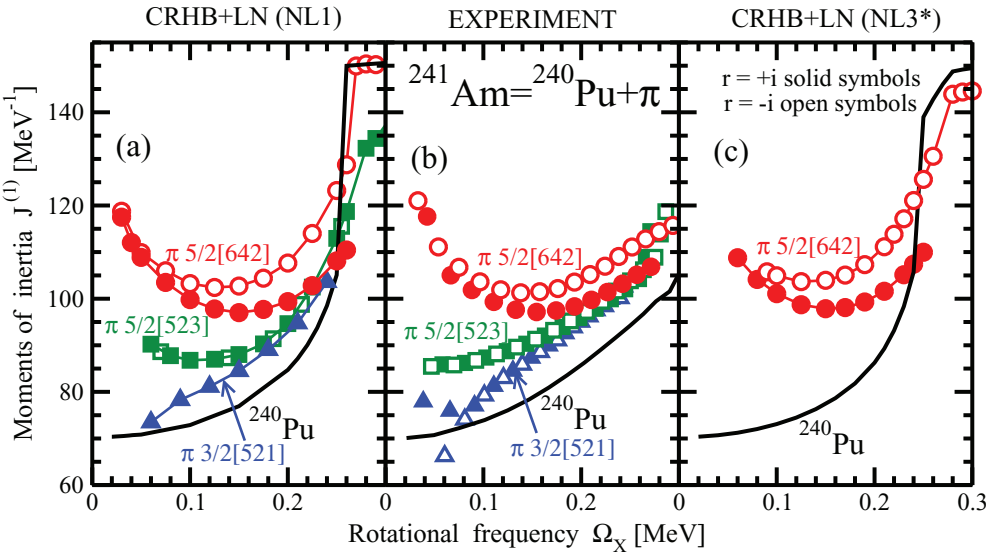

FIG. 16. (Color online) Calculated and experimental kinematic moments of inertia $J^{(1)}$ of the indicated one-quasiproton configurations in the ^{241}Am nucleus and ground-state rotational band in the reference even-even ^{240}Pu nucleus. Experimental data are shown in the middle panel, while the results of the CRHB + LN calculations with the NL1 and NL3* parametrizations are shown in the left and right panels, respectively. The same symbols/lines are used for the same theoretical and experimental configurations. The symbols are used only for the configurations in odd-mass nucleus; the ground-state rotational band in the reference even-even nucleus is shown by the solid black line. The label with the structure "Odd nucleus = reference even+even nucleus + proton(π)/neutron(ν)" is used in order to indicate the reference even-even nucleus and the type of the particle (proton or neutron) active in odd-mass nucleus. The experimental data are from Refs. [94,99].

1. The ^{241}Am nucleus

The rotational bands based on the Nilsson orbitals $\pi 5/2[642]$ (from the $i_{13/2}$ spherical subshell), $\pi 5/2[523]$ (from the $h_{9/2}$ subshell), and $\pi 3/2[521]$ (from the $f_{7/2}$ subshell) have been observed in this nucleus. As can be seen in Fig. 16(b), at low frequencies they have distinctly different kinematic moments of inertia $J^{(1)}$. Theoretical calculations [Figs. 16(a) and 16(c)] describe well the absolute values of the kinematic moments of inertia of different configurations and their evolution with rotational frequency. In particular, the splitting of two signatures of the $\pi 5/2[642]$ configuration is well described in the model calculations. The results of the CRHB + LN(NL1) and CRHB + LN(NL3*) calculations for this configuration are similar.

On the contrary, the $\pi 5/2[523]$ and $\pi 3/2[521]$ bands show (with the exception of very low frequencies in the case of the $\pi 3/2[521]$ band) no signature splitting. The CRHB + LN(NL1) calculations for the two signatures of the $\pi 5/2[523]$ configuration show explicitly this feature. Unfortunately, it was not possible to get a convergence in the case of the $\pi 3/2[521](r = +i)$ configuration. However, the analysis of the quasiparticle routhian diagram confirms that the $\pi 3/2[521](r = \pm i)$ configurations have to be degenerate in energy up to rotational frequency $\Omega_x \sim 0.16$ MeV in agreement with experimental observations. At higher frequencies, small signature separation is expected in the calculations.

In addition to the above-mentioned features, the relative properties of different bands both with respect to each other and with respect to the ground-state band in the reference nucleus ^{240}Pu are well described in the model calculations. The increase of the kinematic moment of inertia in the bands of ^{241}Am as compared with the one of ground-state band in ^{240}Pu is caused by the blocking effect which results in a decreased proton pairing (see Fig. 17).

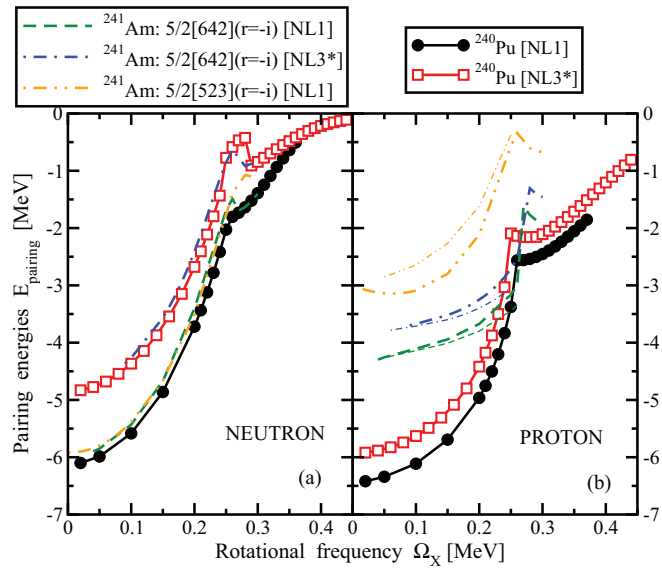

FIG. 17. (Color online) Calculated proton and neutron pairing energies in ground-state rotational band of ^{240}Pu and one-quasiparticle rotational bands of ^{241}Am. Thick and thin lines are used for the $(r = -i)$ and $(r = +i)$ branches of one-quasiparticle configurations, respectively. Note that neutron pairing almost does not depend on the signature of blocked proton orbital. As a result, only the $(r = -i)$ branches are shown in panel (a).

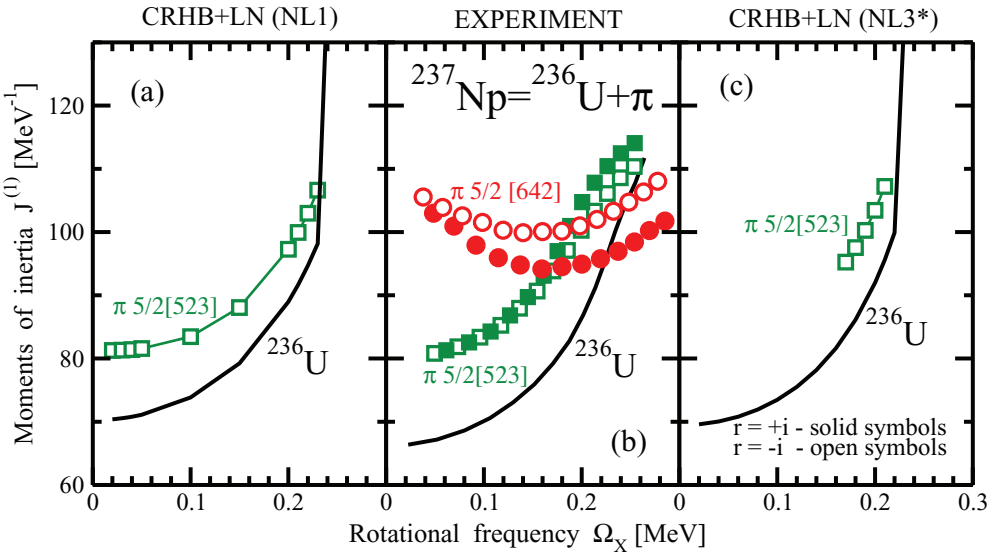

FIG. 18. (Color online) The same as in Fig. 16 but for ^{237}Np. The experimental data are from Ref. [99].

2. *The ^{237}Np nucleus*

Similarly to ^{241}Am, the $\pi 5/2[642]$ and $\pi 5/2[523]$ rotational bands have been observed in this nucleus. Unfortunately, it was possible to obtain a convergent solution only for the $\pi 5/2[523](r = -i)$ configuration (Fig. 18). This configuration rather well describes both its experimental counterpart and the relative properties of the $\pi 5/2[523](r = -i)$ band in ^{237}Np and ground-state band in ^{236}U. The CRHB + LN(NL1) and CRHB + LN(NL3*) results are very similar for this configuration. In the quasiparticle routhian diagram, the $\pi 5/2[523](r = \pm i)$ orbitals are degenerate in energy up to rotational frequency $\Omega_x \sim 0.15$ MeV with small signature separation developing at higher frequencies. These features agree with experimental observations.

3. *The ^{251}Md nucleus*

The $\pi 1/2[521](r = -i)$ configuration has been assigned to the single decoupled band observed recently in the odd-proton nucleus ^{251}Md [104]. In the CRHB + LN(NL1) calculations, this configuration accurately describes both its experimental counterpart and the relative properties of the $\pi 1/2[521](r = -i)$ band in ^{251}Md and the ground-state band in ^{250}Fm [Figs. 19(a) and 19(b)]. On the contrary, it somewhat underestimates experimental $J^{(1)}$ values and the difference between the $J^{(1)}$ values of the $\pi 1/2[521](r = -i)$ band in ^{251}Md and the ground-state band in ^{250}Fm [Figs. 19(b) and 19(c)] in the CRHB + LN(NL3*) calculations.

The results of the CRHB + LN(NL1) calculations for this configuration obtained using an average scaling factor

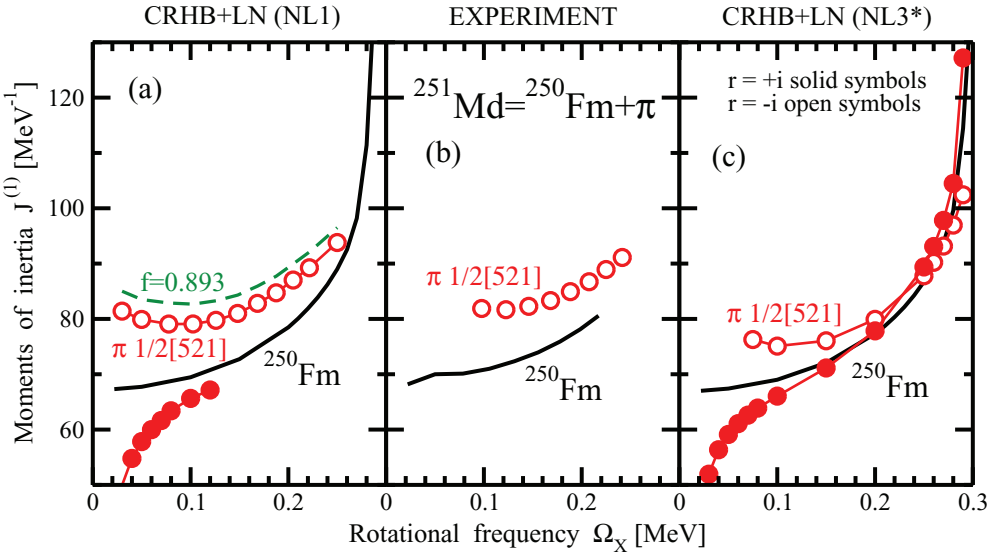

FIG. 19. (Color online) The same as in Fig. 16 but for ^{251}Md. Experimental data are taken from Refs. [65,104].

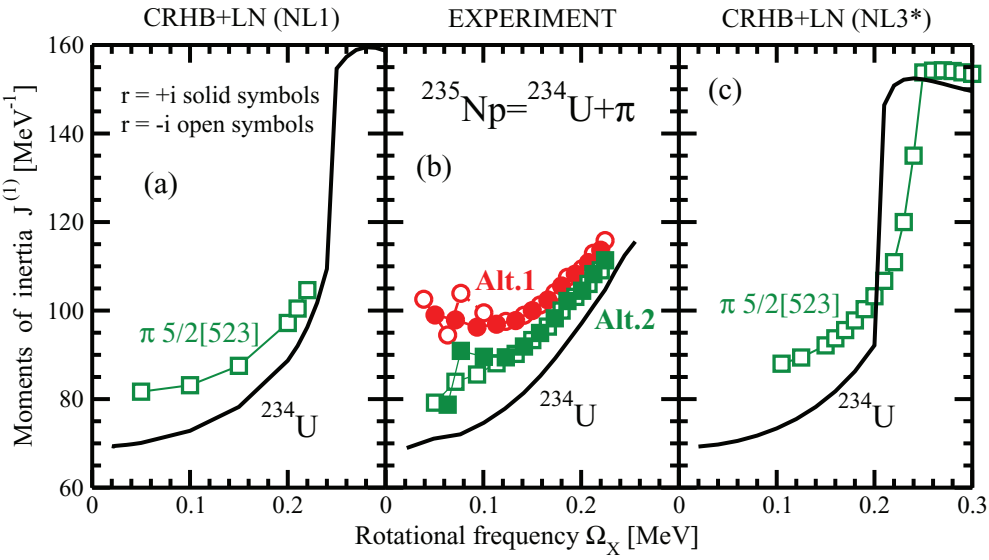

FIG. 20. (Color online) The same as in Fig. 16 but for ^{235}Np. Experimental data are taken from Ref. [105]. See text for details.

$f_{\rm av} = 0.9147$ defined in the current manuscript (open red circles) are compared with the ones (dashed green line) obtained employing the scaling factor $f = 0.893$ of Ref. [1] in Fig. 19(a). One can see that the results of the calculations are very sensitive to the actual value of f; the modification of the scaling factor by 2% leads to visible changes in the calculated $J^{(1)}$ values but does not change much the slope of calculated $J^{(1)}$ curve.

Note that the CRHB + LN(NL1) calculations of Ref. [3] for ^{251}Md have been performed with $f = 0.893$. These calculations showed that the $\pi 7/2[633]$, $\pi 3/2[521]$, $\pi 9/2[624]$, and $\pi 9/2[505]$ configurations cannot be theoretical counterparts of the observed decoupled band because they lead either to signature degenerate bands or to the bands with small signature splitting. As a consequence, both signatures are expected to be observed in experiment.

4. The ^{235}Np nucleus

Two rotational sequences, presumably the two signatures of the ground-state band, have been observed in Ref. [105]. The authors of this reference proposed the $\pi 5/2[624]$ configuration for this band. Figure 20(b) shows the kinematic moments of inertia of these two sequences by solid and open red circles under spin/parity assignments of Ref. [105]; these curves are labeled "Alt. 1." The origin of the disturbances visible at low frequency in the $J^{(1)}$ values of the $r = -i$ sequence is not clear. However, these two sequences are signature degenerate above $\Omega_x \geqslant 0.1$ MeV. This is in clear contrast with the behavior of the $\pi 5/2[624]$ bands in ^{237}Np [Fig. 18(b)] and ^{241}Am [Fig. 16(b)], the two signatures of which show substantial signature splitting. The signature splitting is usually a robust fingerprint of the configuration. In addition, the removal of two neutrons from ^{237}Np should not change the signature splitting in the proton $\pi 5/2[642]$ band since this process will not change the deformation substantially. Because of these two reasons, we believe that the $\pi 5/2[642]$ configuration assignment is not well justified.

The $\pi 5/2[523]$ configuration has also been mentioned as a possible (but less likely) candidate for observed band in Ref. [105]. The $\pi 5/2[523]$ band is signature degenerate in ^{241}Am [Fig. 16(b)], but it develops small signature splitting at high spin in ^{237}Np [Fig. 18(b)]. From our point of view, the $\pi 5/2[523]$ configuration assignment for observed band in ^{235}Np is more likely than the assignment of the $\pi 5/2[642]$ configuration because of the reasons discussed below. However, such reassignment would require the modification of the level scheme in ^{235}Np which is not prohibited since there is neither firm evidence for the lowest member of each rotational sequence nor firm parity assignment [105]. Thus, we suggest the following modifications. The (78)-keV transition linking the $9/2^+$ and $5/2^+$ states in the sequence labeled as 1 in Fig. 5 of Ref. [105] as well as the $5/2^+$ state have to be dropped from the level scheme and the spins of observed states have to be lowered by $1\hbar$ (so the sequence 1 runs from $I^\pi = 7/2^-$ up to $I^\pi = 51/2^-$). The spins of the states in sequence 2 must also be lowered by $1\hbar$, so this sequence runs from $I^\pi = 5/2^-$ up to $I^\pi = 49/2^-$. With these modifications, this band looks very similar to the $\pi 5/2[523]$ band in ^{237}Np shown in Fig. 1 of Ref. [99].

The kinematic moments of inertia of observed sequences under these spin/parity changes are shown by open and closed green squares in Fig. 20(b); these curves are labeled "Alt.2." One can see that this alternative is rather well described by the $\pi 5/2[523](r = -i)$ configuration both in terms of absolute $J^{(1)}$ values and their evolution with spins (Fig. 20). In addition, the relative properties of the bands in ^{235}Np and ^{234}U are rather well reproduced in model calculations. Unfortunately, it was not possible to obtain an opposite signature configuration in the model calculations. However, the analysis of the routhian diagrams in ^{235}Np and the results of the calculations for the $\pi 5/2[523](r = \pm i)$ configurations in ^{241}Am (Fig. 16) suggest that the latter configurations should

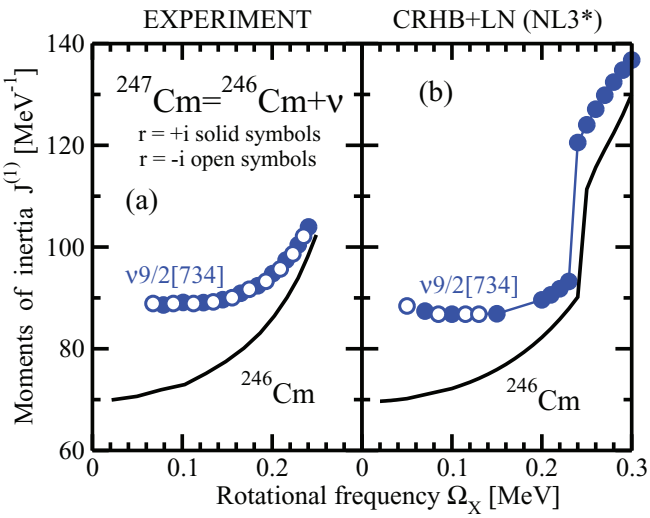

FIG. 21. (Color online) The same as in Fig. 16 but for ^{247}Cm. Experimental data are taken from Ref. [87].

either be signature degenerate or have small signature splitting in ^{235}Np.

B. Odd-neutron nuclei

Long rotational bands based on different single-particle orbitals have been observed in odd-neutron ^{237}U, ^{239,243}Pu, ^{247,249}Cm, ^{249}Cf, and ^{253}No nuclei. Considering that the experimental systematics for odd-neutron systems is larger than that for odd-proton ones, the discussion of the former systems is performed here on a "band-by-band" basis.

1. *The ν9/2[734] rotational band*

This band has been observed in ^{247}Cm, ^{249}Cf, and ^{253}No. Figures 21–23 show the comparison between theory and experiment for it. In all three nuclei, the signature degeneracy of observed band is well reproduced.

In ^{247}Cm, the CRHB + LN(NL3*) calculations accurately reproduce the relative properties of the $\nu 9/2[734]$ band and the reference band in ^{246}Cm. The absolute $J^{(1)}$ values of experimental band are well described up to $\Omega_x \sim 0.15$ MeV (Fig. 21). However, the calculations underestimate the increase of $J^{(1)}$ seen at higher frequencies. This is due to the fact that the increase of $J^{(1)}$ with rotational frequency is underestimated in the reference ^{246}Cm ground-state band. The CRHB + LN(NL3*) calculations accurately reproduce the absolute $J^{(1)}$ values of the $\nu 9/2[734]$ band in ^{249}Cf and their evolution with frequency as well as its relative properties (at low frequency) with respect to the reference band in ^{248}Cf (Fig. 22).

The CRHB + LN(NL1) calculations reproduce very well the $\nu 9/2[734]$ band in ^{253}No and its relative properties with respect to the ground-state band in ^{252}No [Figs. 23(a) and 23(b)]. Similar accuracy of the reproduction of the $\nu 9/2[734]$ band in ^{253}No is achieved in the CRHB + LN(NL3*) calculations at $\Omega_x \geqslant 0.12$ MeV [Figs. 23(b) and 23(c)]. However, at lower frequencies these calculations do not reproduce the increase of the $J^{(1)}$ moments with decreasing Ω_x.

2. *The ν1/2[631] rotational band*

This band has been observed in ^{237}U and ^{239}Pu (Figs. 24 and 25). There is a large separation between the $J^{(1)}$ values corresponding to the $(r = \pm i)$ branches of the $\nu 1/2[631]$ band at low frequency which gradually decreases and finally vanishes at high frequency. This feature and the fact that the $(r = -i)$ branch has lower values of $J^{(1)}$ at low frequency are rather well reproduced in the model calculations. In experiment, the $J^{(1)}$ values in the odd-mass nucleus are higher than the ones in the reference band of the even-even nucleus. However, this difference is underestimated in the model calculations (see Figs. 24 and 25).

3. *The ν7/2[743] rotational band*

This band has been observed in ^{237}U (Fig. 24). It is signature degenerate at low rotational frequencies. A small separation between the $J^{(1)}$ values of the $(r = \pm i)$ branches is seen at medium and high frequencies; at these frequencies, the $(r = +i)$ branch has larger $J^{(1)}$ values. These features are well reproduced in the model calculations with both CDFT parametrizations. The model calculations also reproduce the absolute $J^{(1)}$ values and their evolution with frequency as well as their relative properties with respect to the reference band in ^{236}U. However, the increase of $J^{(1)}$ in the band crossing region is sharp in model calculations but more gradual in experiment. This is similar to the situation seen in the reference ^{236}U nucleus. As discussed in Sec. IV, this discrepancy between theory and experiment in ^{236}U may be due to the stabilization of octupole deformation at high spin which leads to the delay of the alignment of the proton $\pi i_{13/2}$ and neutron $\nu j_{15/2}$ orbitals. If that is the case in nature, a similar situation can be expected also in ^{237}U.

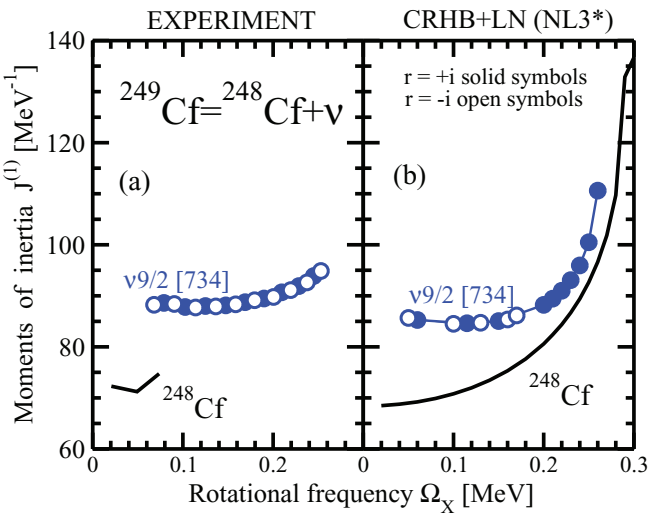

FIG. 22. (Color online) The same as in Fig. 16 but for ^{249}Cf. Experimental data are taken from Ref. [87].

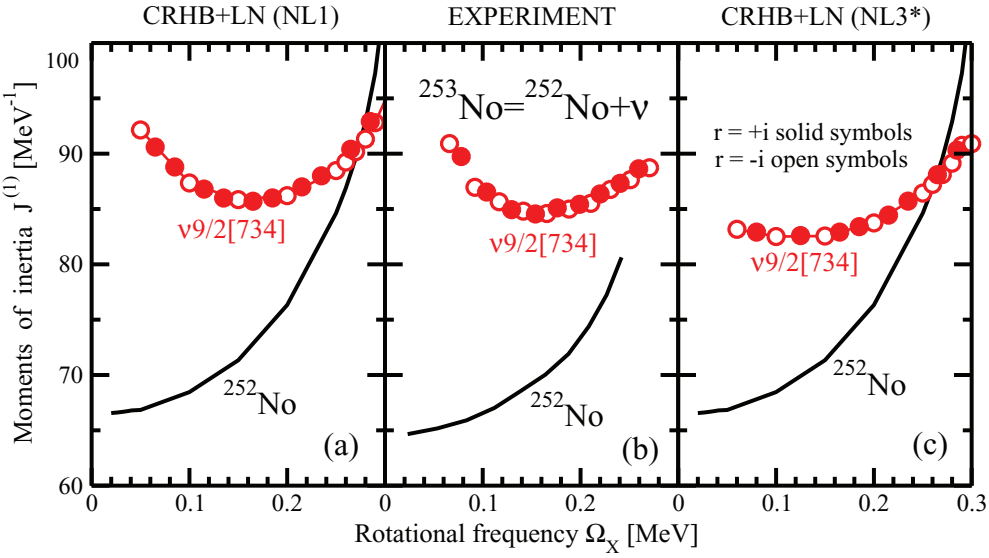

FIG. 23. (Color online) The same as in Fig. 16 but for ^{253}No. Experimental data are taken from Refs. [66,72].

4. The ν5/2[622] rotational band

This band has been observed in ^{237}U (Fig. 24). It is signature degenerate and this feature is reproduced in the CRHB + LN(NL1) calculations. Only the $r = +i$ branch of this band has been obtained in the CRHB + LN(NL3*) calculations. However, the $\pi 5/2[523](r = \pm i)$ orbitals are signature degenerate in the frequency range of interest in the quasiparticle routhian diagram obtained with the NL3* parametrization. The absolute values of $J^{(1)}$ and their evolution with frequency are reproduced in model calculations. The NL1 parametrization somewhat better reproduces the properties of this band with respect to the reference band in ^{236}U than the NL3* parametrization, which underestimates the increase of the $J^{(1)}$ values due to blocking of the $\nu 5/2[622](r = \pm i)$ orbitals.

5. The ν7/2[624] rotational band

This band has been observed in ^{243}Pu (Fig. 27) and it is the only odd-mass nucleus band in the whole actinide region in which a sharp upbend is observed. The model calculations reproduce the properties of this band extremely well, including the absolute $J^{(1)}$ values and their evolution with rotational frequency, signature degeneracy of the $(r = \pm i)$ branches, the relative properties of this band, and the reference band in ^{242}Pu and the properties in the band crossing region. In experiment, the band crossing in the $\nu 7/2[624]$ band takes place earlier (by 0.01 MeV) than the one in the ground-state rotational band of the reference ^{242}Pu nucleus [Fig. 27(b)]. However, in the CRHB + LN(NL1) calculations, both crossings take place at the same frequency [Fig. 27(a)].

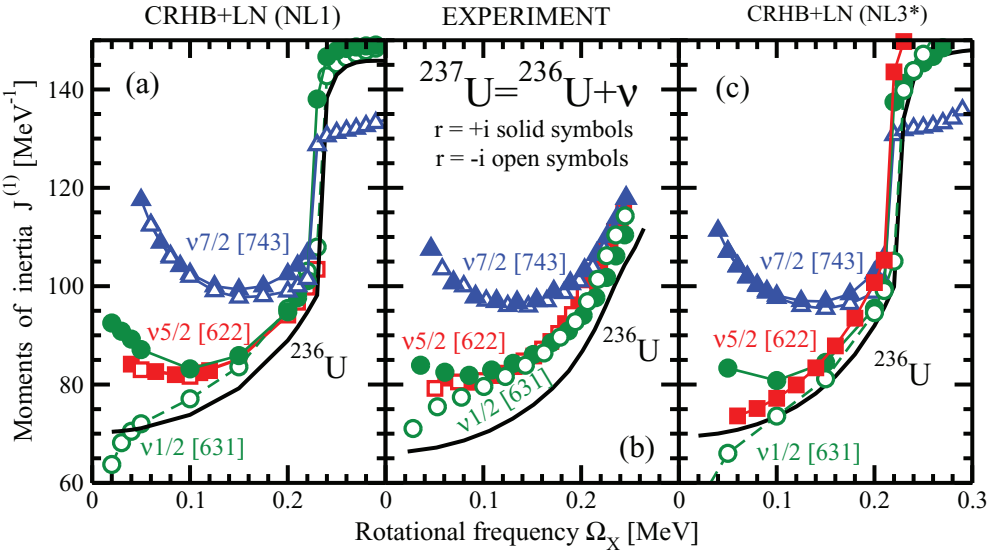

FIG. 24. (Color online) The same as in Fig. 16 but for ^{237}U.

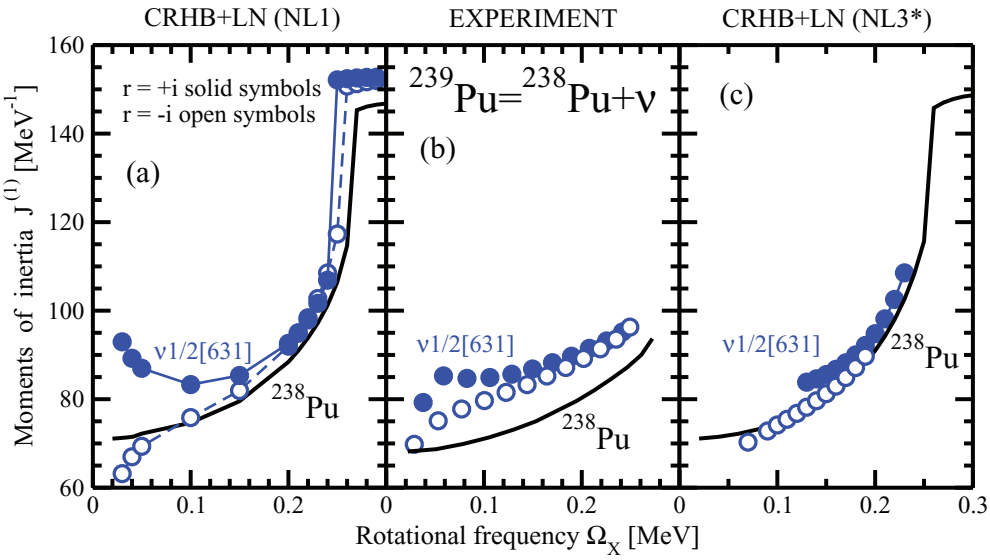

FIG. 25. (Color online) The same as in Fig. 16 but for ^{239}Pu.

6. *The ν1/2[620] rotational band*

This band has been observed in ^{249}Cm (Fig. 26). It was possible to obtain only the $(r = +i)$ branch of the $\nu 1/2[620]$ configuration and only in the CRHB + LN(NL3*) calculations. The slope of experimental $J^{(1)}$ curve as a function of frequency is reasonably well reproduced before the band crossing. However, the relative properties of this band and the ground-state band in the reference ^{248}Cm nucleus are not completely reproduced. Dependent on frequency the $J^{(1)}$ values of the former band are somewhat larger (or similar) than that (to that) of the latter band in experiment. However, the opposite situation is seen in the calculations. The band crossing region is reproduced in general in the calculations. However, in experiment the band approaches the band crossing point in a more gradual way than in the calculations.

C. Rotational properties as a tool of configuration assignment

Ongoing experimental investigations of odd-mass light superheavy nuclei at the edge of the region where spectroscopic studies are still feasible (the nuclei with masses $A \sim 255$ and proton number $Z \geqslant 102$) [3] require reliable theoretical tools for the assignment of one-quasiparticle configurations. This is due to inherent restrictions of the studies at the limits of experimental capabilities. Rotational properties have been occasionally used for that purpose. However, it becomes possible to reliably estimate theoretical errors of the description of rotational properties of such nuclei and the robustness of the configuration assignments based on such properties only by the completion of this systematic study of the odd-mass nuclei.

Indeed, rotational properties of one-quasiparticle configurations yield important information on their underlying structure, thus providing an extra tool for configuration assignment.

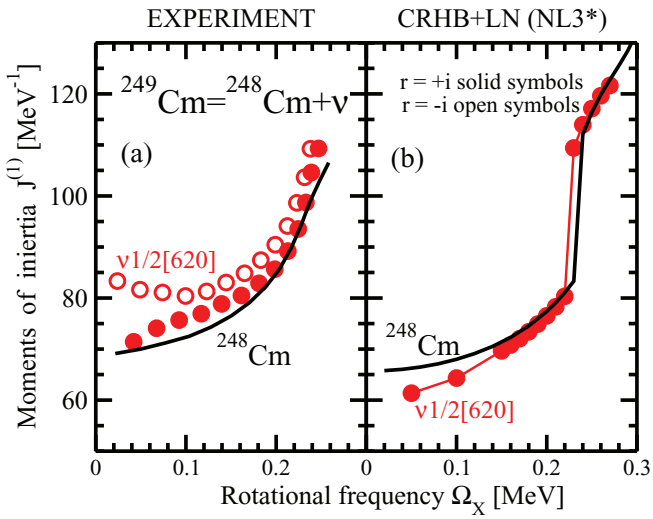

FIG. 26. (Color online) The same as in Fig. 16 but for ^{249}Cm. Experimental data are taken from Ref. [87].

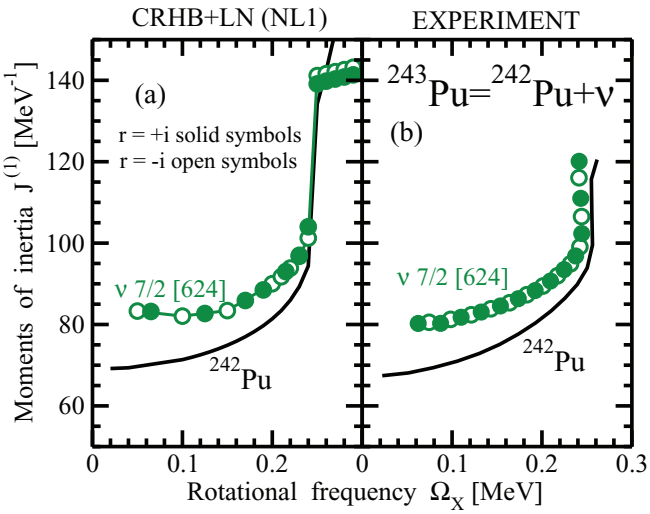

FIG. 27. (Color online) The same as in Fig. 16 but for ^{243}Pu.

The rotational properties are reflected through the following fingerprints

(a) the presence or absence of signature splitting,

(b) the relative properties of different configurations with respect to each other and/or with respect to the ground-state band in the reference even-even nucleus,

(c) the absolute values of the kinematic moments of inertia (especially at low rotational frequencies) and their evolution with rotational frequency.

These fingerprints provide useful tools for quasiparticle configuration assignments. Our systematic investigation shows that with few exceptions these features of rotational bands are well described in model calculations. The presence or absence of signature separation and its magnitude is the most reliable fingerprint which is reproduced in model calculations with good accuracy. The moments of inertia and their evolution with frequency are generally well described in model calculations. As a consequence, the relative properties of different configurations with respect to each other and/or with respect to the ground-state band in the reference even-even nucleus provide a reasonably reliable fingerprint of configuration. This fingerprint is especially useful at low frequencies where the largest difference between the configurations is observed. The calculations fail to describe their relative properties with respect to the reference band in the even-even nucleus only in the cases of the $\nu 1/2[631]$ and $\nu 1/2[620]$ configurations.

However, it is necessary to recognize that the configuration assignment based on rotational properties has to be complemented by other independent methods and has to rely on sufficient experimental data. This is because such a method of configuration assignment does not always leads to a unique candidate configuration due to theoretical inaccuracies in the description of the moments of inertia. The interpretation of the rotational band in ^{253}No is quite illustrative in this respect. Initially, it was interpreted as based on the $\nu 7/2[624]$ configuration [106]. However, improved experiments have allowed us to identify the $M1$ transitions between opposite signatures of the observed band [66] which then led to the $\nu 9/2[734]$ configuration assignment. The kinematic moments of inertia of the observed band under two configuration assignments are described within a typical theoretical uncertainty and, as a result, the configuration assignment based only on rotational properties cannot be fully reliable. The branching ratios of observed $M1$ and $E2$ transitions have to be used in order to distinguish different configuration assignments [66].

VI. ROTATIONAL AND DEFORMATION PROPERTIES OF FISSION ISOMERS

The investigation of fission isomers provides valuable information on rotational and pairing properties in the superdeformed (SD) minimum of actinides. The latter is important for an understanding of fission barriers which sensitively depend on pairing properties (see Ref. [33] and references therein). Although some attempts were made in the 1970s to extract the information on pairing properties at fission saddles [109], they did not lead to reliable estimates. Thus, fission isomers provide the only available tool to estimate the evolution of pairing with deformation in actinides. Such an estimate is available only through the study of rotational properties of ^{236,238}U and ^{240}Pu nuclei; these are the only nuclei for which SD rotational bands were experimentally measured.[3] Although fission isomers in actinides have been observed since the early 1960s, their rotational and single-particle properties are significantly less known experimentally than in other regions of superdeformation. For example, no reliable experimental data on single-particle states in odd-mass actinides exist.

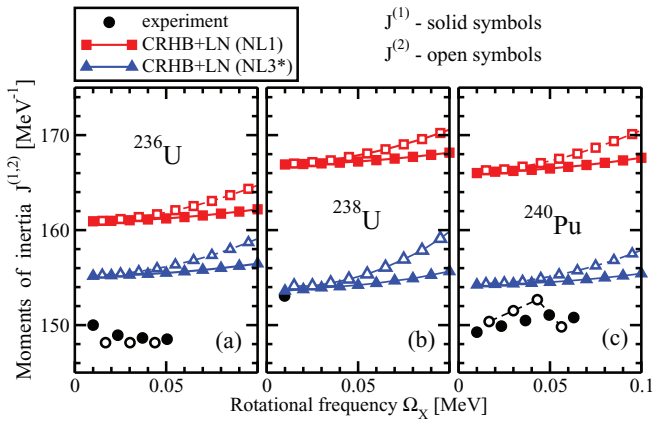

FIG. 28. (Color online) Experimental and calculated kinematic ($J^{(1)}$) and dynamic ($J^{(2)}$) moments of inertia of SD rotational bands in ^{236,238}U and ^{240}Pu. The notation of the lines and symbols is given in the figure.

The experimental and calculated kinematic and dynamic moments of inertia of the SD rotational bands in ^{236,238}U and ^{240}Pu are shown in Fig. 28. The calculated kinematic and dynamic moments of inertia increase with increasing rotational frequency Ω_x (Fig. 1). In addition, the difference between these moments grows with the increase of Ω_x since $J^{(2)}$ rises faster than $J^{(1)}$. In the calculations, these features are predominantly due to gradual alignment of the $N = 8$ neutrons and $N = 7$ protons and a smooth decrease of pairing correlations with increasing Ω_x. They are similar to the ones observed in the $A \sim 190$ region of superdeformation; see Ref. [13] and references therein.

The experimental data in ^{240}Pu shows such features for $J^{(1)}$ and $J^{(2)}$. However, the highest $J^{(2)}$ point deviates from this trend most likely due to the fact that the energy of the $10^+ \rightarrow 8^+$ transition has been measured with lower accuracy than that of other transitions within the SD band [68]. On the other hand, such features are not seen in ^{236}U. This again can be related to insufficient accuracy of the measurements of the γ-transition energies in the SD band of ^{236}U; these energies in the SD bands of ^{236}U and ^{240}Pu are measured with typical accuracy of 1.0 and 0.1 keV, respectively [68].

[3]The information on pairing cannot be extracted from odd-even mass staggerings in the SD minimum, since the inaccuracies of the measurements of excitation energies of fission isomers in odd-mass nuclei are at least 200 keV but can reach 400 keV [108].

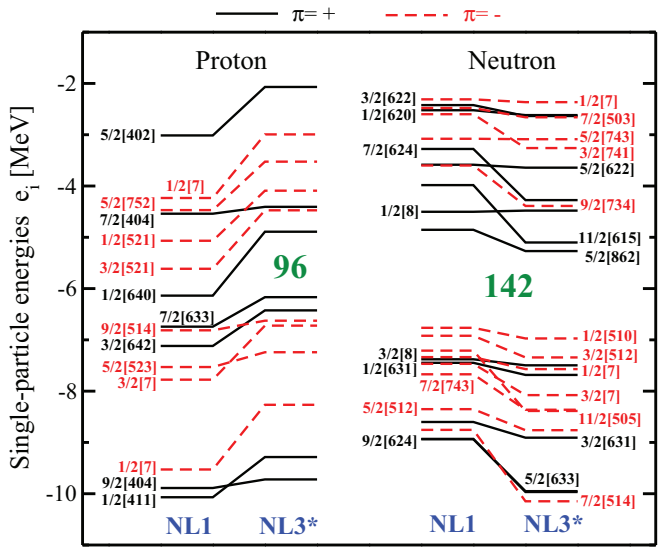

FIG. 29. (Color online) The single-particle levels in the superdeformed minimum of ^{236}U obtained in the calculations with the NL1 and NL3* parametrizations. They are labeled by the Nilsson labels $\Omega[Nn_z\Lambda]$ when the squared amplitude of the dominant component of the wave function exceeds 0.5. Otherwise, the states are labeled by $\Omega[N]$, where N represents the dominant principal quantum number.

The experimental kinematic moments of inertia are best described by the NL3* parametrization; the deviation from experiment does not exceed 3.4% (Fig. 28). Note that similar to low-spin results in the ND minimum (see Sec. III B), the minor variations in the experimental $J^{(1)}$ values with particle number are not reproduced. The fact that the moments of inertia of rotational structures in two different minima (ND and SD) are accurately described with the same pairing strength strongly suggests that the evolution of pairing correlations with deformation is properly described in the CRHB + LN(NL3*) framework by the Brink-Booker part of the Gogny D1S force. This is important for the investigation of fission barriers, the properties of which sensitively depend on the pairing interaction employed [33].

However, this is not always the case, since the CRHB + LN(NL1) calculations substantially overestimate the experimental moments of inertia in the SD minimum [for example, by 11.3% in ^{240}Pu] (Fig. 28) while they reproduce the low-spin moments of inertia in the ND minimum with the same level of accuracy as the CRHB + LN(NL3*) calculations (see Fig. 2). It turns out that reasonable description of the moments of inertia at SD can be achieved in the CRHB + LN(NL1) calculations only if the original strength of the Brink-Booker part of the Gogny D1S force (scaling factor $f = 1.0$) is used in the calculations (see Fig. 1 in Ref. [111]). This clearly indicates that even the pairing force carefully fitted to experimental data at normal deformation does not guarantee accurate description of pairing at SD (and as a consequence also at fission saddle). The origin of such behavior is not completely clear but the difference between the CRHB + LN(NL3*) and CRHB + LN(NL1*) results for $J^{(1)}$ at SD may also partially originate from the differences in the single-particle structures at superdeformation obtained with the NL3* and NL1 parametrizations (Fig. 29). While the large $N = 142$ SD shell gap exists in both parametrizations, a somewhat smaller $Z = 96$ SD shell gap is seen only in the NL3* parametrization (Fig. 29). In addition, the ordering of the single-particle levels differs in these two parametrizations.

Table II shows that for a specific parametrization the calculated pairing energies in the ND and SD minima are comparable in a given subsystem (proton or neutron). They are typically within 0.5 MeV. The only exception is the proton subsystem for which the pairing energies in the SD minimum are larger than those in the ND one by 1.4 MeV. Note that the pairing is stronger in the NL1 parametrization. In part, this is a consequence of the fact that the average scaling factor $f_{\rm av}$ is larger for the NL1 parametrization (see Sec. III B).

The calculated charge quadrupole moments Q are compared with available experimental data in Table I. One should note that the small error bars on the experimental values of Q given for ^{238}U and ^{240}Am nuclei should be treated with caution since even modern experiments do not provide an accuracy of the absolute Q values better than 15%; see the discussion in Ref. [13]. In addition, when comparing the calculations with experiment, one should take into account that (i) the $Q^{\rm exp}$ values have been obtained with different experimental techniques [109] and (ii) it is reasonable to expect that an addition of one neutron to ^{239}Pu will not change the Q value considerably, and, thus, $Q^{\rm exp}(^{239}{\rm Pu})$ could be used for comparison with the calculated $Q(^{240}{\rm Pu})$.

With these considerations in mind, it is clear that the CRHB + LN(NL3*) results come reasonably close to experiment. The CRHB + LN(NL1) results are also not far away from experimental data but they substantially overestimate the experimental Q value in ^{238}U. The Q values obtained in the CRHB + LN(NL1) calculations are always higher than the ones for CRHB + LN(NL3*), which also may be a reason why the CRHB + LN(NL1) calculations systematically overestimate kinematic moments of inertia at SD.

TABLE I. Experimental and theoretical charge quadrupole moments Q of SD fission isomers. The results of the CRHB + LN calculations with the NL1 and NL3* parametrizations are presented. Experimental data for the U and Pu isotopes are taken from Ref. [109], while that for ^{242}Am is from Ref. [110].

	^{236}U	^{238}U	^{236}Pu	^{239}Pu	^{240}Pu	^{242}Am
$Q^{\rm exp}$ (eb)	32 ± 5	29 ± 3	37 ± 10	36 ± 4		$35.5 \pm 1.0_{\rm st} \pm 1.2_{\rm mod}$
$Q^{\rm NL1}$ (eb)	35.8	37.3	36.1		38.2	
$Q^{\rm NL3*}$ (eb)	33.9	33.7	34.8		34.9	

TABLE II. Averaged pairing energies $E^{\nu/\pi}_{\text{pairing}}$ (in MeV) [Eq. (11)] in the normal- (ND) and superdeformed (SD) minima for the NL3* and NL1 parametrizations. These quantities are averaged over ^{236,238}U and ^{240}Pu nuclei; the individual pairing energies in each of these nuclei do not deviate from averaged ones by more than 0.5 MeV.

Parametrization	Neutron		Proton	
	ND	SD	ND	SD
NL3*	4.99	5.51	6.56	6.90
NL1	6.26	6.52	6.97	8.35

The systematic analysis of low-spin properties of the yrast SD bands presented in Fig. 30 is performed with the NL3* parametrization since it describes better available experimental data on deformation and rotational properties of fission isomers. The Q values generally increase with increasing proton number. For a given isotope chain they stay nearly constant in the $N = 142$–150 range. There is a gradual increase of Q at $N > 150$ in the Cm, Cf, and Fm isotopes. In the Th, U, and Pu isotopes, the Q values drop by 5–7 eb on going from $N = 142$ to $N = 140$ [Fig. 30(a)]. This change in equilibrium deformation of the second minimum as a function of neutron number is clearly visible in the deformation energy curves obtained in the RMF+BCS calculations with monopole pairing and the NL3* parametrization (Fig. 7 in Ref. [37]). It is caused by the changes in the underlying shell structure; this is supported by the fact that the RMF+BCS calculations of Ref. [37] with monopole pairing and the current CRHB + LN(NL3*) calculations with the Brink-Booker part of the Gogny D1S force in the pairing channel bring similar values for equilibrium deformation in second minimum despite different treatments of pairing.

The evolution of the kinematic moments of inertia $J^{(1)}$ of the yrast SD bands at low spin as a function of proton and neutron numbers closely resembles the one of charge quadrupole moments Q (Fig. 30). This is mostly due to the fact that the values of kinematic moments of inertia of the SD bands in the limit of no pairing are typically close to the rigid-body values [28] and, thus, are strongly defined by the deformation properties. The pairing lowers the calculated kinematic moments of inertia but does not remove this connection.

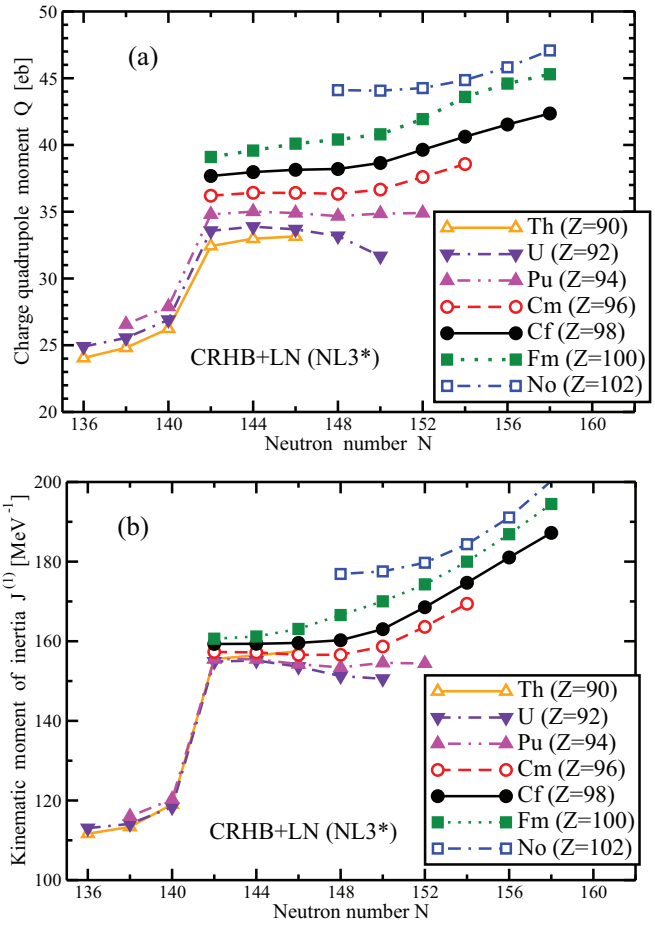

FIG. 30. (Color online) Charge quadrupole moments Q [panel (a)] and kinematic moments of inertia $J^{(1)}$ [panel (b)] of the yrast SD bands as a function of neutron number N. The results are obtained in the CRHB + LN(NL3*) calculations at $\Omega_x = 0.01$ MeV.

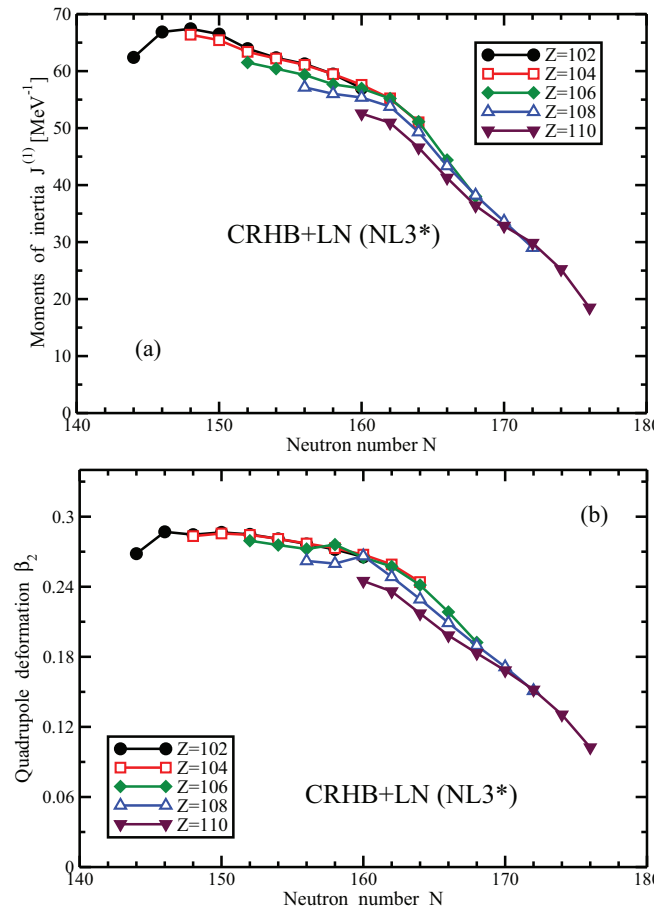

FIG. 31. (Color online) Kinematic moments of inertia [panel (a)] of ground-state bands of superheavy nuclei calculated at $\Omega_x = 0.02$ MeV and their quadrupole deformations β_2 [panel (b)] as a function of neutron number N.

VII. DEFORMATION AND ROTATIONAL OF SUPERHEAVY NUCLEI

Figure 31 shows the calculated quadrupole deformations β_2 and kinematic moments of inertia $J^{(1)}$ of even-even superheavy nuclei with $Z = 102, 104, 106, 108$, and 110 as a function of neutron number N. The nuclear region selected roughly corresponds to the one where superheavy nuclei either have already been measured or may be experimentally studied (including rotational properties) within the next one or two decades. We do not extend our studies to higher Z values since in these nuclei the potential energy surfaces in the normal-deformed minimum become very soft (see Refs. [55,112]), so a description on the mean-field level may not be adequate and the methods beyond mean field [113,114] may be required.

The CRHB + LN calculations of Fig. 31 are performed with the NL3* parametrization. However, earlier investigations of the Fm ($Z = 100$) isotope and $N = 152$ isotone chains in Ref. [1] show that the general trends of the evolution of the $J^{(1)}$ and β_2 quantities as a function of neutron and proton numbers only weakly depend on the CDFT parametrization (see Figs. 13 and 14 in Ref. [1]). Figure 31 shows that calculated quadrupole deformation β_2 stays more or less constant for the neutron numbers $N \leqslant 162$. However, at higher N it decreases gradually with increasing neutron number. The evolution of calculated kinematic moments of inertia correlates strongly with the one for the quadrupole deformations. Indeed, with the exception of the lightest $Z = 102$ nuclei, the $J^{(1)}$ values decrease very slowly with increasing neutron number, but above $N = 162$ the rate of the decrease of $J^{(1)}$ becomes substantially larger.

VIII. CONCLUSIONS

The cranked relativistic Hartree-Bogoliubov theory has been applied for a study of actinides and light superheavy nuclei. The systematic investigation of rotational properties of even-even and odd-mass nuclei at normal deformation has been performed for the first time in the density functional theory framework. In addition, the pairing properties have been systematically studied via the $\Delta^{(3)}$ indicators for the first time in the CDFT theory. The main results can be summarized as follows:

(i) In order to reproduce the moments of inertia in actinides and light superheavy nuclei, the strength of the Brink-Booker part of the Gogny D1S force in the particle-particle channel of the CRHB + LN theory has to be attenuated by $\approx$10%. With this attenuation, the moments of inertia below band crossings and the $\Delta^{(3)}$ indicators are well reproduced. In contrast, the moments of inertia of lighter nuclei with $A \leqslant 200$ are well described with the original strength of the Brink-Booker part of the Gogny D1S force in the CRHB + LN calculations.

(ii) The strengths of pairing defined by means of the moments of inertia and three-point $\Delta^{(3)}$ indicators strongly correlate. This is a known result in non-self-consistent models based on phenomenological Woods-Saxon or Nilsson potentials. However, this is a nontrivial result in the DFT framework since time-odd mean fields (absent in phenomenological potentials) strongly affect the moments of inertia [28] and have an impact on three-point $\Delta^{(3)}$ indicators [26].

(iii) The definitions of pairing strength via these two observables are complimentary. This is because (i) it is difficult to disentangle proton and neutron contributions to pairing when considering the moments of inertia and (ii) the $\Delta^{(3)}$ indicators are affected by particle-vibration coupling and depend on correct reproduction of the ground states in odd-mass nuclei (see Sec. III E for details).

(iv) The calculations with approximate particle number projection by means of the Lipkin-Nogami method provide a better description of the absolute values and particle number dependencies of the moments of inertia as compared with the calculations which do not include it. Similar improvement is observed for the $\Delta^{(3)}$ indicators. However, more systematic calculations of the $\Delta^{(3)}$ indicators in the CRHB + LN and CRHB frameworks are needed to make this observation conclusive.

(v) Sharp upbendings observed in a number of rotational bands of the $A \geqslant 242$ nuclei are well described in the model calculations. The calculations also predict similar upbendings in lighter nuclei but they have not been seen in experiment. The analysis suggests that the stabilization of octupole deformation at high spin, not included in the present CRHB + LN calculations, can be responsible for this discrepancy between theory and experiment.

(vi) The proper description of the evolution of pairing with deformation implies an accurate reproduction of the moments of inertia of rotational structures in normal- and superdeformed minima with the same strength of pairing. This condition is satisfied only in the CRHB + LN(NL3*) calculations. On the contrary, the strength of pairing in the SD minimum has to be increased by almost 10% as compared with the ND minimum in order to reproduce the moments of inertia of the SD bands in the CRHB + LN(NL1) calculations. This clearly indicates that even the pairing force carefully fitted to experimental data at normal deformation does not always guarantee accurate description of pairing at SD (and, as a consequence, also at the fission saddle). The origin of such behavior is not completely clear but partially may be related to the dependence of the shell structure at SD on the parametrization.

(vii) It is well known that the present generation of the density functional theories do not provide the same accuracy of the description of the energies of the single-particle states as the models based on the phenomenological Woods-Saxon or Nilsson potentials (see Ref. [41] and references therein). This is despite the fact that many aspects of the single-particle motion, such as deformation polarization effects due to particle(s)/hole(s) and the impact of the particle(s)/hole(s)

on angular-momentum alignments/moments of inertia, are well described in the DFT models in the regime of no or weak pairing [49,115]. The current systematic study of rotational bands in odd-mass nuclei confirms for the first time this observation also for the pairing regime. This is because, with few exceptions, the impact of the particle on the rotational properties of the bands in odd-mass nuclei is well described in model calculations. As a consequence, the absolute and relative properties of different configurations/bands in odd-mass nucleus with respect to each other and/or with respect to the ground-state band in the reference even-even nucleus provide a reasonably reliable indication of the underlying one-quasiparticle configuration of rotational band in odd-mass nucleus.

ACKNOWLEDGMENTS

The authors thank S. Frauendorf, R. Herzberg, R. V. F. Janssens, T. L. Khoo, and P. Ring for valuable discussions and suggestions. This work was supported by the US Department of Energy under the Grant No. DE-FG02-07ER41459. This research was also supported by an allocation of advanced computing resources provided by the National Science Foundation. The computations were partially performed on Kraken at the National Institute for Computational Sciences (http://www.nics.tennessee.edu/).

[1] A. V. Afanasjev, T. L. Khoo, S. Frauendorf, G. A. Lalazissis, and I. Ahmad, Phys. Rev. C **67**, 024309 (2003).
[2] R. D. Herzberg and P. T. Greenlees, Prog. Part. Nucl. Phys. **61**, 674 (2008).
[3] A. V. Afanasjev, H. Abusara, E. Litvinova, and P. Ring, J. Phys.: Conf. Series **312**, 092004 (2011).
[4] P. Reiter *et al.*, Phys. Rev. Lett. **82**, 509 (1999).
[5] P. T. Greenlees *et al.*, Phys. Rev. Lett. **109**, 012501 (2012).
[6] H. L. Liu, F. R. Xu, and P. M. Walker, Phys. Rev. C **86**, 011301(R) (2012).
[7] Z.-H. Zhang, J.-Y. Zeng, E.-G. Zhao, and S.-G. Zhou, Phys. Rev. C **83**, 011304(R) (2011).
[8] Z.-H. Zhang, X.-T. He, J.-Y. Zeng, E.-G. Zhao, and S.-G. Zhou, Phys. Rev. C **85**, 014324 (2012).
[9] M. Bender, P.-H. Heenen, and P.-G. Reinhard, Rev. Mod. Phys. **75**, 121 (2003).
[10] D. Vretenar, A. V. Afanasjev, G. A. Lalazissis, and P. Ring, Phys. Rep. **409**, 101 (2005).
[11] B. Gall, P. Bonche, J. Dobaczewski, H. Flocard, and P.-H. Heenen, Z. Phys. **348**, 183 (1994).
[12] A. Valor, J. L. Egido, and L. M. Robledo, Nucl. Phys. A **665**, 46 (2000).
[13] A. V. Afanasjev, P. Ring, and J. König, Nucl. Phys. A **676**, 196 (2000).
[14] A. V. Afanasjev and S. Frauendorf, Phys. Rev. C **71**, 064318 (2005).
[15] C. D. O'Leary, C. E. Svensson, S. G. Frauendorf, A. V. Afanasjev, D. E. Appelbe, R. A. E. Austin, G. C. Ball, J. A. Cameron, R. M. Clark, M. Cromaz, P. Fallon, D. F. Hodgson, N. S. Kelsall, A. O. Macchiavelli, I. Ragnarsson, D. Sarantites, J. C. Waddington, and R. Wadsworth, Phys. Rev. C **67**, 021301(R) (2003).
[16] P. J. Davies *et al.*, Phys. Rev. C **75**, 011302(R) (2007).
[17] J. L. Egido and L. M. Robledo, Nucl. Phys. A **570**, 69 (1994).
[18] M. Anguiano, J. L. Egido, and L. M. Robledo, Nucl. Phys. A **683**, 227 (2001).
[19] M. Anguiano, J. L. Egido, and L. M. Robledo, Nucl. Phys. A **696**, 467 (2001).
[20] T. Duguet, P. Bonche, and P.-H. Heenen, Nucl. Phys. A **679**, 427 (2001).
[21] M. Bender, P. Bonche, T. Duguet, and P.-H. Heenen, Nucl. Phys. A **723**, 354 (2003).
[22] *Extended Density Functionals in Nuclear Structure Physics*, Vol. 641 of Lecture Notes in Physics, edited by G. A. Lalazissis, P. Ring, and D. Vretenar (Springer-Verlag, Heidelberg, 2004).
[23] T. D. Cohen, R. J. Furnstahl, and D. K. Griegel, Phys. Rev. C **45**, 1881 (1992).
[24] M. Bender, K. Rutz, P.-G. Reinhard, J. A. Maruhn, and W. Greiner, Phys. Rev. C **60**, 034304 (1999).
[25] E. V. Litvinova and A. V. Afanasjev, Phys. Rev. C **84**, 014305 (2011).
[26] A. V. Afanasjev and H. Abusara, Phys. Rev. C **81**, 014309 (2010).
[27] A. V. Afanasjev and P. Ring, Phys. Rev. C **62**, 031302(R) (2000).
[28] A. V. Afanasjev and H. Abusara, Phys. Rev. C **82**, 034329 (2010).
[29] A. V. Afanasjev, Yue Shi, and W. Nazarewicz, Phys. Rev. C **86**, 031304(R) (2012).
[30] J. J. Valiente-Dobon *et al.*, Phys. Rev. Lett. **95**, 232501 (2005).
[31] M. Serra, A. Rummel, and P. Ring, Phys. Rev. **65**, 014304 (2001).
[32] M. Serra and P. Ring, Phys. Rev. C **65**, 064324 (2002).
[33] S. Karatzikos, A. V. Afanasjev, G. A. Lalazissis, and P. Ring, Phys. Lett. B **689**, 72 (2010).
[34] Y. Tian, Z. Y. Ma, and P. Ring, Phys. Lett. B **676**, 44 (2009).
[35] T. Gonzalez-Llarena, J. L. Egido, G. A. Lalazissis, and P. Ring, Phys. Lett. B **379**, 13 (1996).
[36] P. Ring, Prog. Part. Nucl. Phys. **37**, 193 (1996).
[37] H. Abusara, A. V. Afanasjev, and P. Ring, Phys. Rev. C **82**, 044303 (2010).
[38] G. F. Bertsch, C. A. Bertulani, W. Nazarewicz, N. Schunck, and M. V. Stoitsov, Phys. Rev. C **79**, 034306 (2009).
[39] A. Mukherjee, Y. Alhassid, and G. F. Bertsch, Phys. Rev. C **83**, 014319 (2011).
[40] A. V. Afanasjev, J. König, P. Ring, L. M. Robledo, and J. L. Egido, Phys. Rev. C **62**, 054306 (2000).
[41] A. V. Afanasjev and S. Shawaqfeh, Phys. Lett. B **706**, 177 (2011).
[42] P. A. Butler and W. Nazarewicz, Rev. Mod. Phys. **68**, 349 (1996).
[43] W. Koepf and P. Ring, Nucl. Phys. A **493**, 61 (1989).
[44] U. Hofmann and P. Ring, Phys. Lett. B **214**, 307 (1988).

[45] P.-G. Reinhard, M. Rufa, J. Maruhn, W. Greiner, and J. Friedrich, Z. Phys. A **323**, 13 (1986).
[46] G. A. Lalazissis, S. Karatzikos, R. Fossion, D. Peña Arteaga, A. V. Afanasjev, and P. Ring, Phys. Lett. B **671**, 36 (2009).
[47] S. Frauendorf (private communication).
[48] A. V. Afanasjev, I. Ragnarsson, and P. Ring, Phys. Rev. C **59**, 3166 (1999).
[49] A. V. Afanasjev, G. Lalazissis, and P. Ring, Nucl. Phys. A **634**, 395 (1998).
[50] A. V. Afanasjev, J. Koenig, and P. Ring, Nucl. Phys. A **608**, 107 (1996).
[51] A. V. Afanasjev and S. Frauendorf, Phys. Rev. C **72**, 031301(R) (2005).
[52] Y. C. Zhang *et al*., Phys. Rev. C **76**, 064321 (2007).
[53] Z. Q. Sheng, Z. Z. Ren, and W. Z. Hang, Nucl. Phys. A **832**, 49 (2010).
[54] T. Gaitanos, A. B. Larionov, H. Lenske, and U. Mosel, Phys. Rev. C **81**, 054316 (2010).
[55] H. Abusara, A. V. Afanasjev, and P. Ring, Phys. Rev. C **85**, 024314 (2012).
[56] B. G. Todd-Rutel and J. Piekarewicz, Phys. Rev. Lett. **95**, 122501 (2005).
[57] S. Typel and H. H. Wolter, Nucl. Phys. A **656**, 331 (1999).
[58] G. A. Lalazissis, T. Nikšić, D. Vretenar, and P. Ring, Phys. Rev. C **71**, 024312 (2005).
[59] B. A. Nikolaus, T. Hoch, and D. G. Madland, Phys. Rev. C **46**, 1757 (1992).
[60] T. Bürvenich, D. G. Madland, J. A. Maruhn, and P.-G. Reinhard, Phys. Rev. C **65**, 044308 (2002).
[61] T. Nikšić, D. Vretenar, and P. Ring, Phys. Rev. C **78**, 034318 (2008).
[62] P. W. Zhao, Z. P. Li, J. M. Yao, and J. Meng, Phys. Rev. C **82**, 054319 (2010).
[63] J. F. Berger, M. Girod, and D. Gogny, Comp. Phys. Comm. **63**, 365 (1991).
[64] J. F. Berger, M. Girod, and D. Gogny, Nucl. Phys. A **428**, 23c (1984).
[65] J. E. Bastin *et al*., Phys. Rev. C **73**, 024308 (2006).
[66] R.-D. Herzberg *et al*., Eur. Phys. J. A **42**, 333 (2009).
[67] H. B. Jeppesen *et al*., Phys. Rev. C **80**, 034324 (2009).
[68] Evaluated Nuclear Structure Data File (ENSDF) located on the Brookhaven National Laboratory website, http://www.nndc.bnl.gov/ensdf/. ENSDF is based on the publications presented in Nuclear Data Sheets (NDS), which is a standard for evaluated nuclear data.
[69] T. Ishii, S. Shigematsu, H. Makii, M. Asai, K. Tsukada, A. Toyoshima, M. Matsuda, A. Makishima, T. Shizuma, J. Kaneko, I. Hossain, H. Toume, M. Ohara, S. Ichikawa, T. Kohno, and M. Ogawa, Phys. At. Nucl. **70**, 1457 (2007).
[70] S. Raman, C. H. Malarkey, W. T. Milner, C. W. Nestor, Jr., and P. H. Stelson, At. Data Nucl. Data Tables **36**, 1 (1987).
[71] L. Grodzins, Phys. Lett. **2**, 88 (1962).
[72] R.-D. Herzberg *et al*., Phys. Rev. C **65**, 014303 (2001).
[73] W. Nazarewicz and I. Ragnarsson, in *Handbook on Nuclear Properties*, edited by D. N. Poenaru and W. Greiner (Claredon Press, Oxford, 1996), p. 80.
[74] J. Dobaczewski, P. Magierski, W. Nazarewicz, W. Satula, and Z. Szymański, Phys. Rev. C **63**, 024308 (2001).
[75] J. L. Egido and L. M. Robledo, Phys. Rev. Lett. **85**, 1198 (2000).
[76] J.-P. Delaroche, M. Girod, H. Goutte, and J. Libert, Nucl. Phys. A **771**, 103 (2006).
[77] M. Warda and J. L. Egido, Phys. Rev. C **86**, 014322 (2012).
[78] S. Hilaire and M. Girod, Eur. Phys. J. A **33**, 237 (2007); see http://www-phynu.cea.fr/science_en_ligne/carte_potentiels_microscopiques/carte_potentiel_nucleaire_eng.htm for a detailed compilation of the results.
[79] L. Bonneau, P. Quentin, and P. Möller, Phys. Rev. C **76**, 024320 (2007).
[80] G. Coló, H. Sagawa, and P. F. Bortignon, Phys. Rev. C **82**, 064307 (2010).
[81] F. A. Gareev, S. P. Ivanova, L. A. Malov, and V. G. Soloviev, Nucl. Phys. A **171**, 134 (1971).
[82] S. P. Ivanova, A. L. Komov, L. A. Malov, and V. G. Soloviev, Izv. Akad. Nauk SSSR Ser. Fiz. **37**, 911 (1973) [Bull. Acad. Sci. USSR, Phys. Ser. (Engl. Transl.) **37**, 3 (1973)].
[83] L. A. Malov (private communication).
[84] S. Hota and P. Chowdhury (private communication).
[85] J. L. Egido and P. Ring, J. Phys. G **8**, L43 (1982).
[86] Y. S. Chen and S. Frauendorf, Nucl. Phys. A **393**, 135 (1983).
[87] S. K. Tandel, P. Chowdhury, S. Lakshmi, U. S. Tandel, I. Ahmad, M. P. Carpenter, S. Gros, R. V. F. Janssens, T. L. Khoo, F. G. Kondev, J. P. Greene, D. J. Hartley, T. Lauritsen, C. J. Lister, D. Peterson, A. Robinson, D. Seweryniak, and S. Zhu, Phys. Rev. C **82**, 041301(R) (2010).
[88] M. Ploszajczak and A. Faessler, J. Phys. G **8**, 709 (1982).
[89] J. L. Egido and P. Ring, Nucl. Phys. A **423**, 93 (1984).
[90] I. Hamamoto, Nucl. Phys. A **271**, 15 (1976).
[91] S. Frauendorf and V. V. Pashkevich, Phys. Lett. B **141**, 23 (1984).
[92] R. V. Jolos, P. von Brentano, and J. Jolie, Phys. Rev. C **86**, 024319 (2012).
[93] S. Frauendorf, Phys. Rev. C **77**, 021304(R) (2008).
[94] X. Wang, R. V. F. Janssens, M. P. Carpenter, S. Zhu, I. Wiedenhöver, U. Garg, S. Frauendorf, T. Nakatsukasa, I. Ahmad, A. Bernstein, E. Diffenderfer, S. J. Freeman, J. P. Greene, T. L. Khoo, F. G. Kondev, A. Larabee, T. Lauritsen, C. J. Lister, B. Meredith, D. Seweryniak, C. Teal, and P. Wilson, Phys. Rev. Lett. **102**, 122501 (2009).
[95] S. Zhu, M. P. Carpenter, R. V. F. Janssens, S. Frauendorf, I. Ahmad, T. L. Khoo, F. G. Kondev, T. Lauritsen, C. J. Lister, and D. Seweryniak, Phys. Rev. C **81**, 041306(R) (2010).
[96] S. Zhu, R. V. F. Janssens, G. J. Lane, I. Wiedenhöver, M. P. Carpenter, I. Ahmad, A. P. Byrne, P. Chowdhury, D. Cline, A. N. Deacon, G. D. Dracoulis, S. J. Freeman, N. J. Hammond, G. D. Jones, T. L. Khoo, F. G. Kondev, T. Lauritsen, C. J. Lister, A. O. Macchiavelli, E. F. Moore, D. Seweryniak, J. F. Smith, and C. Y. Wu, Phys. Lett. B **618**, 51 (2005).
[97] R. K. Sheline and M. A. Riley, Phys. Rev. C **61**, 057301 (2000).
[98] R. V. F. Janssens (private communication).
[99] K. Abu Saleem, R. V. F. Janssens, M. P. Carpenter, F. G. Kondev, I. Wiedenhöver, I. Ahmad, J. Caggiano, P. Chowdhury, J. A. Cizewski, D. Cline, M. Devlin, N. Fotiades, J. P. Greene, G. Hackman, A. Heinz, T. L. Khoo, T. Lauritsen, C. J. Lister, A. O. Macchiavelli, E. H. Seabury, D. Seweryniak, A. Sonzogni, and C. Y. Wu, Phys. Rev. C **70**, 024310 (2004).
[100] J. Terasaki, H. Flocard, P.-H. Heenen, and P. Bonche, Phys. Rev. C **55**, 1231 (1997).

[101] P. Ring, R. Beck, and H. J. Mang, Z. Phys. **231**, 10 (1970).
[102] J. L. Egido, H. J. Mang, and P. Ring, Nucl. Phys. A **334** 1 (1980).
[103] P. Ring and P. Schuck, *The Nuclear Many-Body Problem* (Springer-Verlag, Heidelberg, 1980).
[104] A. Chatillon *et al*., Phys. Rev. Lett. **98**, 132503 (2007).
[105] A. M. Hurst, C. Y. Wu, M. A. Stoyer, D. Cline, A. B. Hayes, S. Zhu, M. P. Carpenter, K. Abu Saleem, I. Ahmad, J. A. Becker, C. J. Chiara, J. P. Greene, R. V. F. Janssens, T. L. Khoo, F. G. Kondev, T. Lauritsen, C. J. Lister, G. Mukherjee, S. V. Rigby, D. Seweryniak, and I. Stefanescu, Phys. Rev. C **81**, 014312 (2010).
[106] P. Reiter *et al*., Phys. Rev. Lett. **95**, 032501 (2005).
[107] H. C. Britt and J. R. Huizenga, Phys. Rev. C **9**, 435 (1974).
[108] B. Singh, R. Zywina, and R. B. Firestone, Nucl. Data Sheets **97**, 241 (2002).
[109] D. Habs, Nucl. Phys. A **502**, 105c (1989).
[110] H. Backe, M. Hies, H. Kunz, W. Lauth, O. Curtze, P. Schwamb, M. Sewtz, W. Theobald, R. Zahn, K. Eberhardt, N. Trautmann, D. Habs, R. Repnow, and B. Fricke, Phys. Rev. Lett. **80**, 920 (1998).
[111] A. V. Afanasjev, G. Lalazissis, and P. Ring, Acta Phys. Hung. N. S. **6**, 299 (1997).
[112] V. Prassa, T. Niksic, G. A. Lalazissis, and D. Vretenar, Phys. Rev. C **86**, 024317 (2012).
[113] M. Bender, P. Bonche, and P.-H. Heenen, Phys. Rev. C **74**, 024312 (2006).
[114] Z. P. Li, T. Niksic, D. Vretenar, J. Meng, G. A. Lalazissis, and P. Ring, Phys. Rev. C **79**, 054301 (2009).
[115] M. Matev, A. V. Afanasjev, J. Dobaczewski, G. A. Lalazissis, and W. Nazarewicz, Phys. Rev. C **76**, 034304 (2007).